THERMOELECTRIC HYBRID PHOTOVOLTAIC SYSTEM FOR ENHANCED CONTROL OF WATER PUMPS

A DISSERTATION SUBMITTED IN THE PARTIAL FULFILLMENT FOR THE DEGREE OF

MASTER OF ENGINEERING
(CONTROL & INSTRUMENTATION)
(2007 – 2009)

Submitted by
ROHIT KUMAR
University Roll No: 12243

Guided by

Dr. VISHAL VERMA
Electrical Engineering Department

Delhi College of Engineering
(University of Delhi)

CERTIFICATE

It is certified that **Mr. Rohit Kumar** , University Roll No. 12243 , student of M.E , control and instrumentation, Department of Electrical Engineering, Delhi College of Engineering, has submitted the dissertation entitled **"THERMOELECTRIC HYBRID PHOTOVOLTAIC SYSTEM FOR ENHANCED CONTROL OF WATER PUMPS"** under my guidance towards partial fulfillment of the requirements for the award of the degree of Master of Engineering (Control & Instrumentation Engineering).

This dissertation is a bonafide record of project work carried out by him under my guidance and supervision. His work is found to be outstanding and has not been done earlier.

I wish him success in all his endeavors.

Dr. Vishal Verma
Electrical Engineering Department
Delhi College of Engineering

ACKNOWLEDGEMENT

I would like to extend my gratitude and thanks to my guide **Dr. Vishal Verma, Electrical Engineering department, Delhi College of Engineering, Delhi** for his valuable guidance, constant encouragement and helpful discussions throughout the course of this work. Obviously the progress I have made now would have been uncertain without his guidance.

I would like to thank **Prof. Parmod Kumar**, Head of the department, Electrical Engineering for providing valuable comments.

Rohit Kumar
College Roll No. 15/C&I/07
University Roll No : 12243

Abstract

Water pumping has a history dating back to the earliest civilizations and many methods have been developed over the years to realize this task with the minimum of effort. Various power sources including human energy, animal power, wind and hydro-power, electrical (grid) power and fossil fuel powered generator/pump pumping sets have been utilised to accomplish this. Photovoltaic powered pumping systems are a relatively recent addition to this list. Photovoltaic water pumping applications are one of the most common uses of PV power throughout the world, with thousands of solar-powered water pumps installed both in industrialised and developing nations. Owing to their inherent low maintenance and high reliability, they are also increasingly being used as a replacement for mechanical windmill pumps. A true fixed orientation, direct-coupled, PV-powered water pumping system typically consists of an energy conversion process (photovoltaic – light to direct current electricity), a transmission medium (wiring), Inverter, controller and a power consumer (motor/pump set). The dominant problems associated with this type of design (direct-coupled PV) are the non-linear supply of power and the resultant complexity in providing an optimised load match. The output from a PV array is a non-linear and time-dependant source of power that changes according to the variation in solar irradiance throughout a day, as well as the attenuating effects of PV cell temperature. This directly influences the performance characteristics of a motor, which is generally designed for, and operated from, a fixed voltage source. In a PV Pumping System (PVPS), a pump driven by a motor performs optimally at a specific PV array configuration and pumping head profile.

The necessity of efficient and reliable energy conversion is a pressing need of todays problems. PV alone amidst thermal insolation does not conform to efficient way of energy conversion and certainly needs good heat sinks to operate efficiently throughout the duration of solar insolation. Hybridization of PV with Thermoelectric modules can increase the overall efficiency of the solar energy conversion system by keeping the temperature constant within limits thus overcoming the detrimental effects of changing temperature on PV cell. For enhanced control of water pumps vector control of motor/pump is used which can work satisfactorily with non-constant power output of Photovoltaic-TE Hybrids with super capacitors or energy storage support.

This thesis is an attempt to explore the efficient means of water pumping through augmentation of thermoelectric conversion to increase overall efficiency of PV array and using vector control induction motor drive for pump operation. A dynamic model of PV array has been developed and simulated under MATLAB environment for operation of vector control induction motor drive. A model of thermoelectric module was also developed in order to study thermoelectric power conversion, its efficiency and its usefulness in hybrid model of PV and Thermoelectric modules. Model of hybrid combination of Thermoelectric – PV array have been developed and simulation results are also presented in the thesis.

List of figures

Chapter 1

Introduction

1.1 Background

Photovoltaics (abbreviated PV) are the most direct way to convert solar radiation into electricity and are based on the photovoltaic effect, which was first observed by Henri Becquerel in 1839. It is quite generally defined as the emergence of an electric voltage between two electrodes attached to a solid or liquid system upon shining light onto this system. Practically

All photovoltaic devices incorporate a pn junction in a semiconductor across which the photo voltage is developed. These devices are also known as solar cells. Light absorption occurs in a semiconductor material. The semiconductor material has to be able to absorb a large part of the solar spectrum. Dependent on the absorption properties of the material, the light is absorbed in a region more or less close to the surface. When light quanta are absorbed, electron hole pairs are generated, and if their recombination is prevented they can reach the junction where they are separated by an electric field. Even for a weakly absorbing semiconductor like silicon, most carriers are generated near the surface. This leads to the typical solar cell structure of Fig. 1.1.

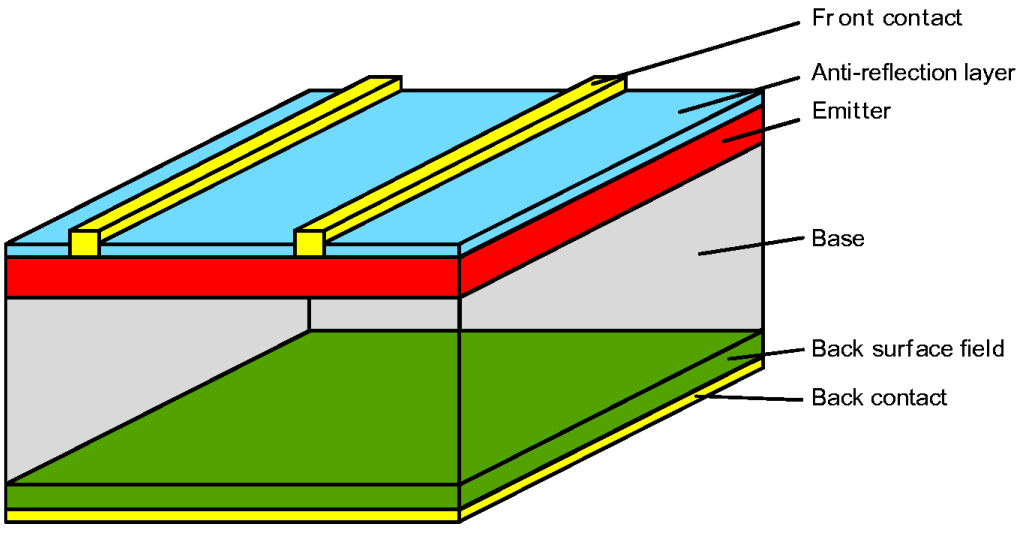

Fig. 1.1. Typical solar cell structure

The pn junction that separates the emitter and base layer is very close to the surface in order to have a high collection probability for the photo generated charge carriers. The thin emitter layer above the junction has a relatively high resistance which requires a well designed contact grid, also shown in the figure. For practical use solar cells are packaged into modules containing either a number of crystalline Si cells connected in series or a layer of thin-film material which is also internally series connected. The module serves two purposes: It protects the solar cells from the ambient and it delivers a higher voltage than a single cell, which develops only a voltage of less than 1Volt. The conversion efficiencies of today's production cells are in the range of 13 to 16%, but module efficiencies are somewhat lower. The best laboratory efficiency of crystalline silicon achieved so far is 24.7%, which approaches the theoretical limit of this type of solar cell.

Technology

The photovoltaic effect remained a laboratory curiosity from 1839 until 1959, when the first silicon solar cell was developed at Bell Laboratories in 1954 by Chapin et al. It already had an efficiency of 6%, which was rapidly increased to 10%. The main application for many years was in space vehicle power supplies. Terrestrial application of photovoltaics (PV) developed very slowly. Nevertheless, PV fascinated not only the researchers, but also the general public. Its strong points are:

– direct conversion of solar radiation into electricity,

– no mechanical moving parts, no noise,

– no high temperatures,

– no pollution,

– PV modules have a very long lifetime,

– the energy source, the sun, is free, ubiquitous, and inexhaustible,

– PV is a very flexible energy source, its power ranging from microwatts to megawatts.

Solar cell technology benefited greatly from the high standard of silicon technology developed originally for transistors and later for integrated circuits This applied also to the quality and availability of single crystal silicon of high perfection As the cost of silicon is a significant proportion of the cost of a solar cell, great efforts have been made to reduce these costs. One technology, which dates back to the 1970s, is block casting which avoids the costly pulling process. Silicon is melted and poured into a square SiO/SiN-coated graphite crucible. Controlled cooling produces a polycrystalline silicon block with a large crystal grain structure .from solid state physics we know that silicon is not the ideal material for photovoltaic conversion. It is a material with relatively low absorption of solar radiation, and, therefore, a thick layer of silicon is required for efficient absorption. Theoretically, this can be explained by the semiconductor band structure of silicon in which the valence band maximum is offset from the conduction band minimum. Since the basic process of light absorption is excitation of an electron from the valence to the conduction band, light absorption is impeded because it requires a change of momentum. The search for a more suitable material started almost with the beginning of solar cell technology. This search concentrated on the thin-film materials. They are characterized by a direct band structure, which gives them very strong light absorption.

Today, the goal is still elusive, although promising materials and technologies are beginning to emerge. The first material to appear was amorphous Silicon (a-Si). It is remarkable that even the second contender in this field is based on the element silicon, this time in its amorphous form. Amorphous silicon has properties fundamentally different from crystalline silicon. However, it took quite some time before the basic properties of the material were understood. The high expectancy in this material was curbed by the relatively low efficiency obtained so far and by the initial light-induced degradation for this kind of solar cell (so-called Staebler–Wronski effect).Today, a-Si has its fixed place in consumer applications, mainly for indoor use. After understanding and partly solving the problems of light-induced degradation, amorphous silicon begins to enter the power market. Stabilized cell efficiencies reach 13%. Module efficiencies are in the 6–8% range. The visual appearance of thin-film modules makes them attractive for facade applications. Beyond amorphous silicon there are many other potential solar cell materials fulfilling the requirement of high light absorption and are therefore suitable for thin-film solar cells.

1.2 The Silicon Solar Cell

The physics of solar cells is most straight forward for crystalline silicon cells. To understand the function of semiconductor devices and thus of solar cells, a precise understanding of the processes within a p-n junction is crucial. The base unit of many semiconductor devices is a semiconductor body, in which two different dopants directly adjoin one another. This is called a p-n junction if a p-doped area merges into an n-doped area within the same lattice. In a simple example, we assume that – in silicon – both dopants are of the same magnitude and merge together abruptly. The left-hand side $x < 0$ would, for example, be doped with boron atoms with a concentration of NA = 1016 atoms per cm−3, making it p-conductive. The right-hand side $x > 0$, on the other hand, could be doped with phosphorus atoms, at ND = 1016 cm−3, making it n-conductive. The freely moving charge carriers will not follow the abrupt change in concentration from NA to ND. Rather, the carriers will diffuse due to the difference in concentration, i.e., the holes from the p region will move into the n region, and the electrons from the n area will move into the p region.

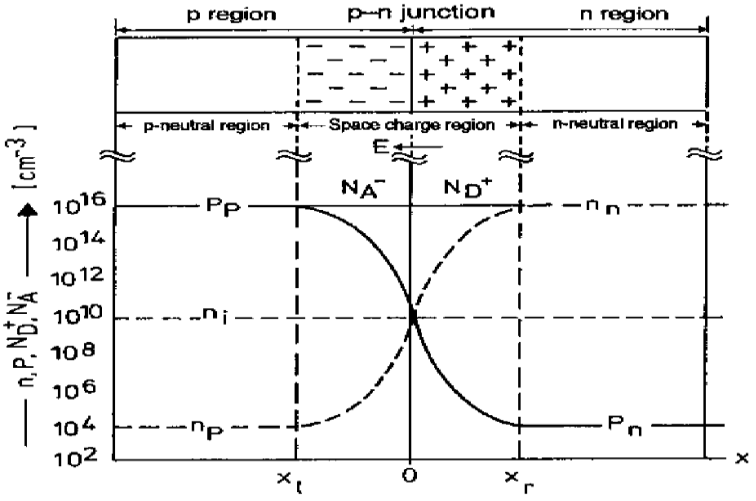

Fig 1.2 Doping and concentration distribution of a symmetrical p-n junction in thermal equilibrium

Diffusion currents will arise. The ionized acceptors and donors, which are no longer electrically compensated, remain behind as fixed space charges (Fig. 1.2). Negative space charges will arise on the left-hand side in the p region, and positive space charges arise on the right-hand side in the n region. Correspondingly – as occurs in a plate capacitor – an electric field is created .

Doping and concentration distribution of a symmetrical p-n junction in thermal equilibrium at the p-n junction, which is directed so that it drives the diffusing charge carriers in the opposite direction to the diffusion. This process continues until an equilibrium is created or, in other words, until the diffusion flow is compensated by a field current of equal magnitude. An (extremely large) internal electric field exists – even if both sides of the semiconductor are grounded. When the p-n junction is illuminated, charge carrier pairs will be generated wherever light is absorbed. The strong field at the junction pulls minority carriers across the junction and a current flow results. The semiconductor device is not in thermal equilibrium, which means that electric power can be delivered to a load. This is the basic mechanism of a solar cell. A typical such solar cell according to Fig. 1.1 consists of a p-n junction, which has a diode characteristic.

This characteristic can be derived from standard solid state physics. It is:

$$I = I_0(\exp (V_A/V_T) - 1), \qquad (1.1)$$

where I is the current through diode at applied voltage V_A. V_T is a constant, the so-called thermal voltage. I_0 is the diode saturation current, which depends on the type, doping density, and quality of the semiconductor material and the quality of the p-n junction. If this junction is illuminated, an additional current, the light-generated current I_L is added:

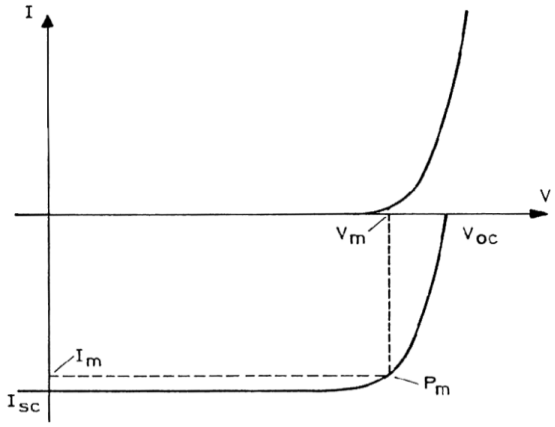

Fig. 1.3 I–V-characteristic of solar cell without (**top**) and with illumination. Vm, Im, and Pm are values at maximum power

$$I = I_0(\exp(V_A/V_T) - 1) - I_L \, . \qquad (1.2)$$

The negative sign in (2.3) results from polarity conventions. Now the current I is no longer zero at zero voltage but is shifted to I_L. Power can be delivered to an electric load. The I/V characteristic with and without illumination is shown in Fig.1.3 This figure also defines three important quantities: Voc, the open circuit voltage, Isc, the short circuit current, which is identical to I_L, and the maximum power point Pm at which the product of V and I is at a maximum. This is the optimal operating point of the solar cell. Voltage and current at Pm are Vm and Im. It is obvious that the ideal solar cell has a characteristic that approaches a rectangle. The fill factor $FF = I$m Vm$/ I$sc Voc should be close to one. For very good crystalline silicon solar cells, the fill factors are above 0.8 or 80%. From (1.2) we can also recognize the importance of the saturation current I_0. The open circuit voltage is obtained when no current is drawn from the cell. Then:

$$V\text{oc} = V_T \ln (I_L/ I_0 + 1) \, . \qquad (1.3)$$

Even at low current densities the term I_L/ I_0 is large compared to 1, so we find that Voc $\approx V_T$ $\ln(I_{sc}/ I_0)$, i.e., the open circuit voltage is proportional to the logarithm of the ratio of I_{sc} to I_0. This means that although I_0 is a very small quantity compared to I_L, lowering the saturation current is very crucial for increasing efficiency. From solar cell physics it can be derived that there are three sources for I_0: a) minority carrier leakage current from the emitter region, b) a minority carrier leakage current from the base region, and c) a space charge recombination current.

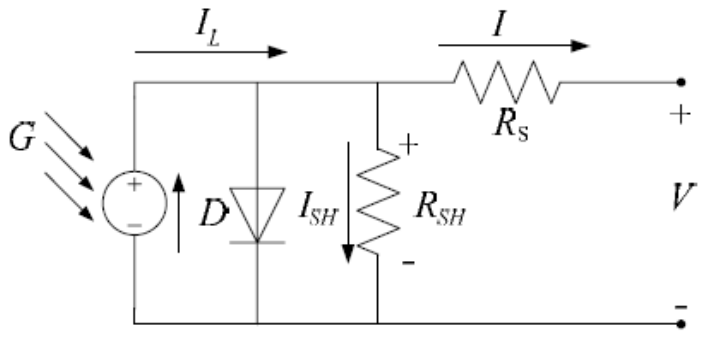

Fig. 1.4. Equivalent circuit of solar cell with diode model

With these components an equivalent circuit of a solar cell can be constructed. It contains all relevant components. These are: a current source due to the light-induced current I_L, and diode saturation currents I_D. The other components are of resistive nature, a parallel (shunt) resistance R_{sh} and a series resistance R_S. Evidently, R_{sh} should be as high and R_S as low as possible. *Efficiency* The conversion efficiency is the most important property of a solar cell. It is defined as the ratio of the photovoltaically generated electric output of the cell to the radiative power falling on it:

$$\eta = I_m V_m / P_{light} = FF\ Isc\ Voc / P_{light} \quad (1.4)$$

where *FF* is the fill factor $V_m I_m / V_{oc} I_{sc}$ Efficiency is measured under standard conditions

1.3 General Configuration for Solar Energy collection System

Terrestrial photovoltaic applications can be divided into:

– stand-alone PV systems and

– grid-connected PV systems.

A comparison of stand-alone PV systems and Grid connected on the world PV market from 1990 to 2002.is given.Clearly, it can be seen that the percentage of the grid-connected increased rapidly during this time .

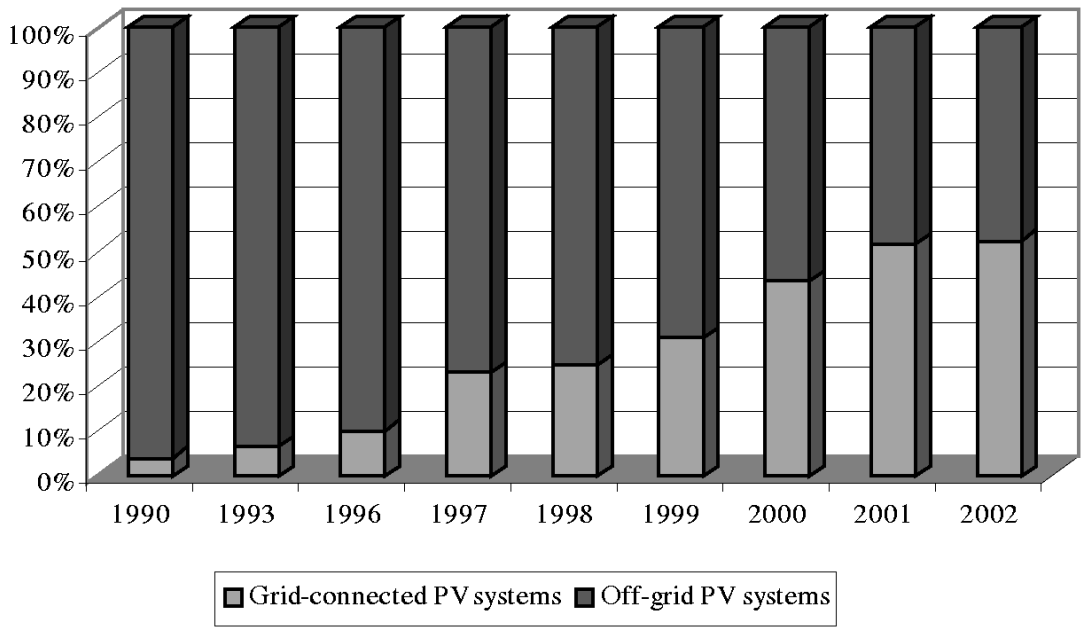

Fig 1.5 Comparison showing growth of grid connected & off grid PV systems

1.3.1 Stand-Alone PV Systems

Stand-alone photovoltaically powered systems with peak PV powers can have from milliwatts to several kilowatts. They do not have a connection to an electricity grid. In order to ensure the supply of the stand-alone system with electric power also in the times without radiation (e.g., at night) or with very market in 2002 low radiation (e.g., at times with a strong cloud cover), stand-alone systems mostly have an integrated storage system. If the systems are used only during the time when the radiation is sufficient to supply the system with electric power directly, a storage system is not necessary.

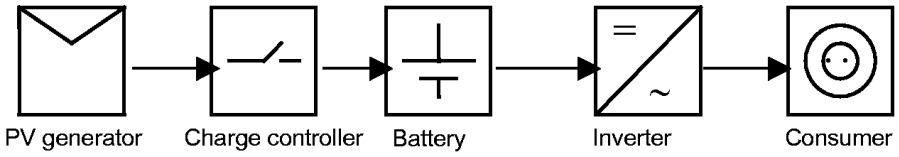

Fig 1.6 Schematic principle of a stand-alone PV system supplying a building

Mostly the internal grid of the house works with AC power. Therefore, the PV system includes one or two inverters. Because the radiation intensity changes with the time of day as well as the season and weather conditions, a stand-alone PV system that is used to supply a building with electrical energy must also have a storage battery and a charge controller. The schematic principle of stand-alone PVsystem supplying a building is given in Fig. 1.6.

Batteries – In most cases, lead-acid batteries are used for this purpose. Recently, some firms began offering so-called solar batteries specifically designed for stand-alone PV systems. It should be stressed that batteries in a PV system operate in a very demanding environment, in particular, seasonal periods with very low charge are encountered. This situation is alleviated in hybrid systems in which the auxiliary generator can charge the battery during such periods.

Charge controller – A PV battery charge controller serves generally to protect the battery against overcharging and deep discharge. It is absolutely necessary for the efficient operating conditions of the battery and of the complete PV system

1.3.2 Hybrid Systems

Because of the annual fluctuation of the solar radiation in most parts of the world, an exclusively photovoltaic power supply system would demand a large solar generator and/or a large storage battery. Such a PV system is very expensive. This also applies to photovoltaic systems for which security of supply is very important. Therefore, usually different types of electricity generators are combined into a so-called hybrid system. A combination of photovoltaic and fossil-fuelled generators guarantees the same supply reliability as the public grid. Under favorable weather conditions, the total energy demand is met by the solar generator. Surplus energy is stored in batteries. During the night or unfavorable weather, the energy demand is initially met by the batteries. If there is danger of deep discharge, a diesel or gas-fuelled generator provides the electricity and simultaneously charges the battery. At windy

sites, the system can include a wind energy converter. As the photovoltaic generator and wind energy converter largely complement each other if they are dimensioned correctly, the operating time of the fossil-fuelled generator, and thus the fuel consumption, are reduced.

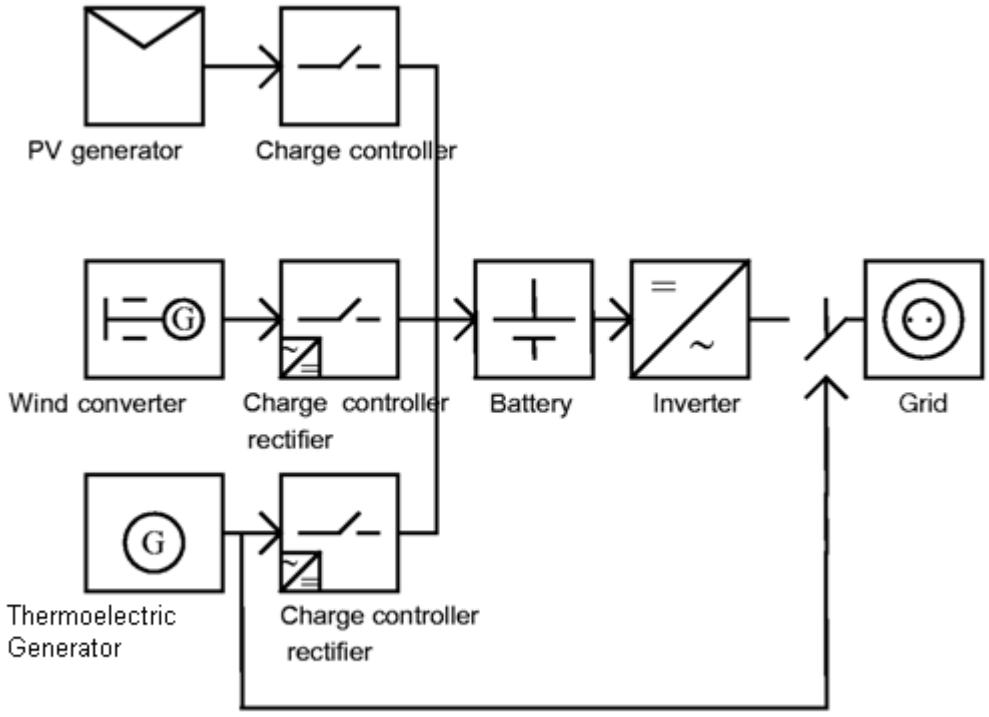

Fig. 1.7 Schematic principle of a hybrid system with PV, wind, and Thermoelectric generators

1.3.3 Grid-Connected PV Systems

Grid-connected PV systems always have a connection to the public electricity grid via a suitable inverter, because a PV module delivers only dc power. Normally there are almost no effects of the PV systems on the grid affecting power quality, load-on lines, and transformers, etc. However, for a larger share of PV in low-voltage grids, as in solar settlements, these

aspects need to be taken into account. From a technical point of view, there will be no difficulty in integrating as much PV into low-voltage grids as the peak load of the respective segment.

Grid-connected PV systems can be subdivided into two kinds:

– decentralized grid-connected PV systems,

– central grid-connected PV systems.

1.3.3.1 Decentralized Grid-Connected PV Systems

Decentralized grid-connected PV systems have mostly a small power range and are installed on the roof of buildings (rooftop or flat-roof installation) or integrated into building facades. Energy storage is not necessary in this case. On sunny days, the solar generator provides power, e.g., for the electrical appliances in the house.

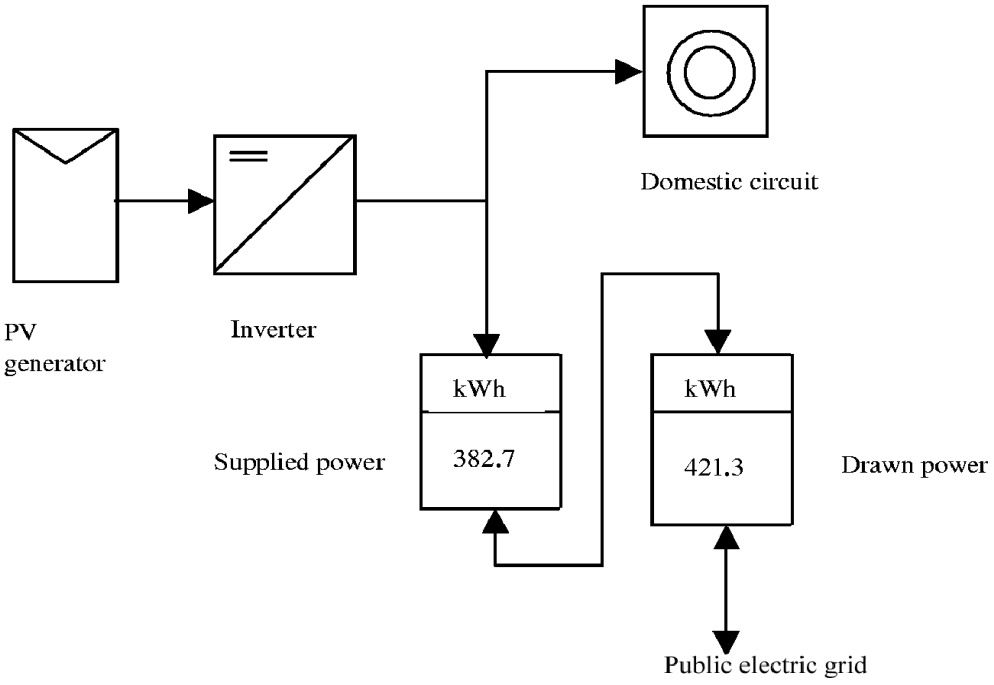

Fig. 1.9 Block diagram of the power supply for a house with a decentralized PV system and grid connection

Excess energy is supplied to the public grid. During the night and overcast days, the house draws its power from grid (Fig. 1.9). In this way, the electricity grid can be regarded as a large "storage unit." In the case of a favorable rate-based tariff for PV electricity, as is in force in some countries, it is more advantageous to feed all solar electricity into the grid.

1.3.3.2 Central Grid-Connected PV Systems

Central grid-connected PV systems have an installed power up to the MW range. With such central photovoltaic power stations it is possible to feed directly into the medium or high voltage grid. Mostly central photovoltaic power stations are set up on otherwise unused land, but in some cases an installation on buildings, mostly on the flat roof of greater buildings, is also possible. As can be seen both decentralized and central grid connected PV systems consist of the following two main components:

– PV module,

– Inverter.

1.3.3 Photovoltaic Water Pumping

PV systems can be used for pumping water for irrigation of land, as well as for pumping drinking water (Fig. 1.8). Often these two possibilities cannot be separated clearly. Water which is pumped for land irrigation can be used as drinking water also. Therefore, PV systems for irrigation and drinking water will be described together. Access to a safe and clean water supply is one of the primary factors in improving the health and quality of life in rural communities. In the developing world, especially in Africa, Asia, and Latin America, a lot of people do not have the option of using clean water for drinking. These remote regions are not connected to a centralized system for supply drinking water. The principal means of water lifting in the developing world are presently the hand pump for smaller demands and the diesel-engine-driven pump for larger quantities. Solar PV pumping can be more appropriate than these technologies in many applications.

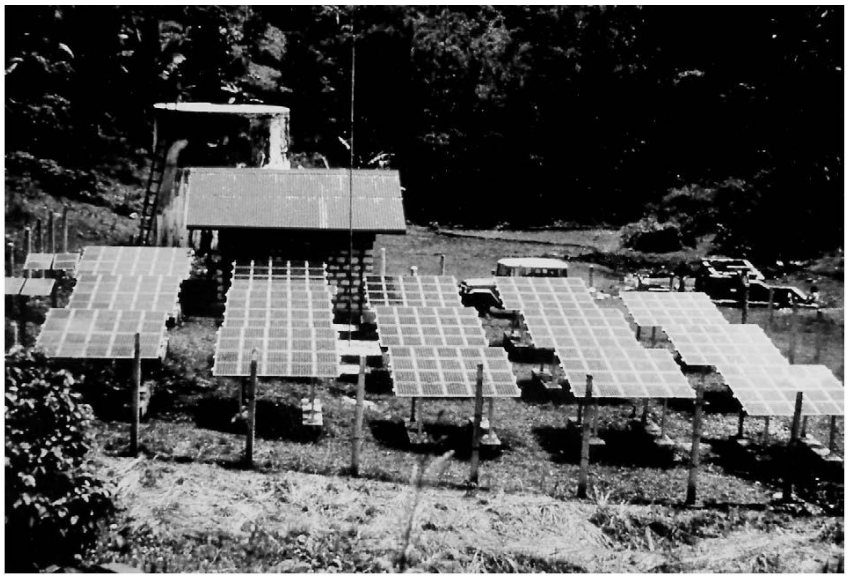

Fig. 1.8 Example of water pumping with PV

In India, more than 5,000 solar PV water pumping systems from various manufacturers are installed. Among these are nearly 300 pumps for drinking water. Small pumping systems with an array capacity of 300–360Wp were developed and tried during the 1980s. In 1993, a new program with higher system capacities was introduced. Under this program, users are offered a combination of grants and soft loans. In a recent initiative, the Ministry of Non-conventional Energy Sources (MNES) provided support to the Punjab Energy Development Agency for deploying 500 solar pumps with a 1,800Wp PV array and a 2 hp DC motor pump set. It is possible to irrigate about 2–3 hectares of land using such solar pumps. Some states in India are planning and implementing larger and larger solar pumping programs, because it is becoming increasingly uneconomical for the state governments to extend the public grid. PV can be useful not only for water pumping, but also for water purification and desalination. Some of the possible methods are listed here:

– micro filtration,

– ultraviolet irradiation, and

– photovoltaically operated Reverse Osmosis (RO) plants.

1.4 Thermoelectric (TEG) conversion

In **1823** Seebeck reported the results of experiments in which a compass needle was deflected if placed in the vicinity of a closed loop, formed from two dissimilar conductors, when one of the junctions was heated. See beck erroneously concluded that the interaction was a magnetic phenomenon and, in pursuing this line of thought, attempted to relate the Earth's magnetism to the temperature difference between the equator and the Poles. Nevertheless, he did investigate the phenomenon in a large number of materials, including some we now call semiconductors, and arranged them in order of the product ***αo,*** where α is the Seebeck coefficient and ***o*** the electrical conductivity. The Seebeck coefficient is expressed in volts per degree, or more often in micro volts per degree μVK^{-I}. The Seebeck series formed in this way is very similar to the present-day thermoelectric series and, had Seebeck employed the first and last members of his series in a thermocouple, he could have converted thermal energy into electricity in **1821** with an efficiency of about **3%,** which compares very favorably with the most efficient steam engine of the day. With the benefit of hindsight it is apparent from Seebeck's account that the phenomenon observed was caused by an electric current flowing in the circuit and that he had discovered the so-called thermoelectric effects.

Some **12** years later, a complementary effect was discovered by Peltier, who observed temperature changes in the vicinity of the junction between dissimilar conductors when a current passed. Although Peltier used the Seebeck effect in his experiments as a source of weak currents, he failed to appreciate the fundamental nature of his observations, or to relate the effect to the findings of Seebeck. The true nature of the Peltier effect was explained by Lenz in **1838.** He concluded that, depending upon the direction of the current flow, heat is absorbed or generated at a junction between two conductors and demonstrated this by freezing water at a bismuth-junction and melting the ice by reversing the direction of current flow.

In **1909** and **1911** Altenkirch gave a satisfactory theory of thermoelectric generation and refrigeration and showed that good thermoelectric materials should possess large Seebeck coefficients with low thermal conductivity (A) to retain the heat at the junction and low electrical resistance to minimize Joule heating. These desirable properties were embodied in a so called figure-of-merit Z, where $Z = \alpha^2\sigma/\lambda$ and the unit of Z is 1/K. At a given absolute temperature T, since Z may vary with T, a useful non dimensional figure-of-merit is ZT.

Although the properties favorable for thermoelectric applications were well known, the important advantages offered by Seebeck's mineral semiconductors were overlooked with the attention of researchers focused on metal and metal alloys. In these materials the ratio of the thermal conductivity to electrical conductivity is a constant (Wiedemann-Franz-Lorenz law) and it is not possible to reduce one while increasing the other. Consequently, the metals best suited are those with the highest Seebeck coefficients. Most metals possess Seebeck coefficients of 10 μVK^{-I} or less, giving associated generating efficiencies of a fraction of 1%, which are uneconomical as a source of electrical power. Similar considerations also led to the conclusion that thermoelectric refrigeration was an uneconomic proposition. Established thermoelectric materials conveniently fall into three categories depending upon their temperature range of operation. **Bismuth telluride** and its alloys have the highest figures-of-merit, are extensively employed in refrigeration, and have a maximum operating temperature of around 450 K. Alloys based on **lead telluride** have the next highest figures-of-merit with silicon germanium alloys having the lowest. Lead telluride and silicon germanium are used in generator applications with upper operating temperatures of around 1000 and 1300 K, respectively.

1.5 State of the Art

Thrust Areas of R & D in Solar Photovoltaic Technology

In order to make solar cells and modules cost effective the global R&D efforts are directed to reduce the consumption of silicon and other materials and improve the efficiency of solar cells / modules to achieve significant cost reduction. Further, R&D is also undertaken on non-silicon based solar cell modules and other aspects of PV systems. it is envisaged that the cost of solar photovoltaic modules can be brought down to about Rs. 120 per Wp. In order to achieve this goal the key areas of R&D and technology development have been identified. Research, design and development efforts during the 11^{th} plan are proposed to be focused on development of

(i) Poly silicon and other materials,

(ii) Efficient silicon solar cells,

(iii) Thin films materials and solar cell modules,

(iv) Concentrating PV systems,

(v) PV system design, with the objective of significantly reducing the ratio of capital cost to conversion efficiency.

Poly Silicon Material

i. To undertake R&D to make poly silicon material using alternative methods to achieve direct electricity consumption of 125 kWh/kg or lower.

Crystalline Silicon Solar Cells & Modules

1. To reduce the direct consumption of silicon wafer (3 gm per Wp) in commercial production by reducing the wafer thickness and increasing the efficiency of crystalline silicon solar cell to average 18% and more.

2. Alternative device structures to make crystalline silicon solar cells to demonstrate very high efficiency (22-24% on small size laboratory devices)

3. Improving the effective PV module life to 30 years and more, with total degradation within 10% of the initial rating under STC.

Thin Film Solar Cell Modules

Thin film solar cell modules have potential to reduce the cost of solar modules due to consumption of less material and energy in the fabrication processes. Amorphous silicon thin film solar cells were the first to be developed. In the recent years pilot plants and a few commercial plants based on other thin film solar cell modules (CdTe, CIGS, silicon) have been set up. It is proposed to take up R&D and pilot plant demonstration of thin film based modules in the country during the 11^{th} plan, with the following objectives.

Laboratory scale small area (2cm x 2cm) devices of efficiency >10% using CdTe, CIGS and silicon thin films are under process. Development of poly crystalline thin film integrated modules (1 sq ft or more) at pilot plant scale using different materials (CdTe, CIGS, silicon films) to achieve efficiency of >8% and life of integrated module > 20 years)

Concentrating Solar Cells & Modules

Apart from the improvements in the performance of flat plate PV modules, it is possible to reduce the material consumption and lower the cost through use of concentrating PV systems. In order to gain experience on performance of the concentrating system and develop systems suitable for use in India, the following activities are proposed during the 11^{th} plan.

1. Design and development of concentrator solar cells (concentration ratio of 200 sun and more) and modules (efficiency ~ 25 – 30%) and testing of concentrating PV system in Indian conditions.

2. Development of two axis tracking system suitable for high concentration PV system.

3. Design and development of heat sink for mounting of solar cells under high concentration

4. Design and development of optical systems to achieve concentration ratio of 200 suns and more, with minimum optical aberration.

5. Development of silicon and GaAs based solar cells suitable for use under high concentration (200 sun or more)

Storage System

At present stand-alone systems use lead acid batteries. However, with low power consuming LED based systems use of NiMH and other similar batteries is also coming up. One of the major constraints in battery storage system is the limited life of storage batteries. There is an urgent need to enhance the battery cycle life to get at least 10 years of operating life. Further, it is also necessary to develop non-lead acid batteries. In addition, alternative methods of storage, especially to store large quantity of power for a few hours would substantially improve the viability of grid interactive PV systems. Development of long life (5000 cycles or more) storage batteries suitable for use in PV systems /applications is under process. Development and testing of new and alternative storage systems up to MW scale. It should be possible to store electricity for about 8-10 hours, with storage losses limited to about 10%.

Balance of System & PV Systems

Design and development of high efficiency (>50%) motor pump set of output power of up to 5 hp to lift water from shallow and deep well (about 30 – 60 meters). Small capacity inverter cum charge controller, with total efficiency of 90% or more, suitable for use in solar lighting systems including LED based lighting systems are also under development. field-testing of inverters and grid synchronizing system components (peak efficiency >96% and part load @ 30% efficiency >88%,) used in residential grid interactive roof top PV systems.

1.6 Motivation

The present work aims to analyze the performance of the water pumps connected to the Hybrid Photovoltaic-TEG systems both during steady state operation and transient operation. Further, it also focuses on the modifications to the conventional architecture and design of the control schemes to improve the performance during abnormal conditions together with its performance evaluation using time domain studies

The main objectives behind the present work are as follows:

To develop mathematical models of TEG & Photovoltaic with its controllers and evaluate its performance during Low insolation conditions using time domain simulations

To propose modifications to the conventional architecture and propose control methods which can improve the performance of the system during unhealthy conditions.

To investigate and present the dynamic performance of the proposed architectures with various configurations of Hybrid system so that overall system efficiency is improved.

1.7 Organisation of Thesis

The thesis has been organized into five chapters. The present chapter introduces very briefly, the various Solar energy schemes and some of the technical challenges with the efficiency improvement and inter connection of grid. It presents the relevant state of art survey and sets the motivation behind the work carried out in the thesis.

Chapter-2, Describes the general literature survey of components of PV –TEG modules and its use for the noble cause of water pumping taking into account the non constant nature of power output from these modules

Chapter-3, Describes the modeling of individual components of PV , Thermoelectric and controllers for pump/motor using MATLAB/Simulink. Controller design is to improve the performance during unhealthy conditions. Study of the integrated system during steady state and transient simulation studies have been presented.

In Chapter-4, a modification to conventional PV system is introduced in which Hybrid PV –TE is used. TE is used for cooling of PV module thus overcoming the detrimental effects of changing temperature on PV cell.

Finally, Chapter-5 presents main findings in the thesis and future scope

Chapter 2

Literature survey of Photovoltaic – Thermoelectric Systems

2.1 Photovoltaic system

The photovoltaic modules are made up of silicon cells. The silicon solar cells which give output voltage of around 0.7V under open circuit condition. When many such cells are connected in series we get a solar PV module. Normally in a module there are 36 cells which amount for a open circuit voltage of about 20V. The current rating of the modules depends on the area of the individual cells. Higher the cell area high is the current output of the cell. For obtaining higher power output the solar PV modules are connected in series and parallel combinations forming solar PV arrays. A typical characteristic curve of the called current (I) and voltage (V) curve and power (W) and voltage (V) curve of the module is shown is shown in Fig.2.1

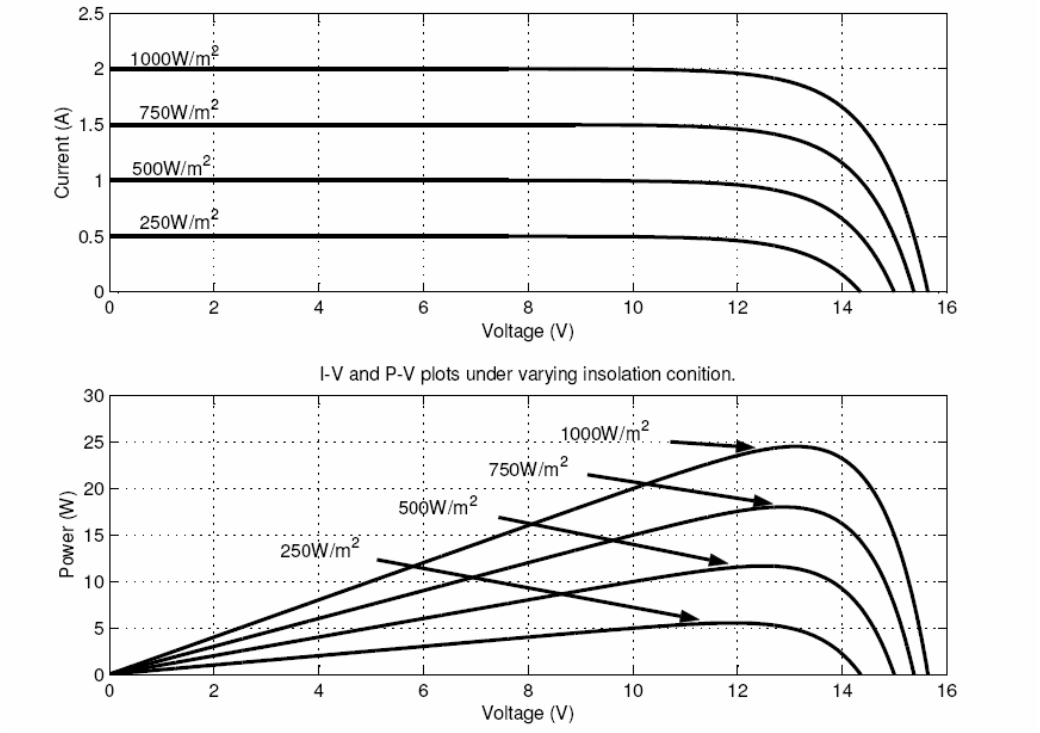

Fig 2.1 I-V and P-V plots under varying insolation condition.

Temperature Effects

Operating temperature has a strong effect on the electrical response of solar cells. Taking into account that in, terrestrial applications, solar cells can easily warm up to 60–65 C and that in space or satellite applications temperatures can be even higher, it follows that a proper modelling of the temperature coefficients of the main electrical parameters is mandatory. Temperature effects in a solar cell can be evaluated by using the built in parameters of the diode model included in the equivalent circuit.

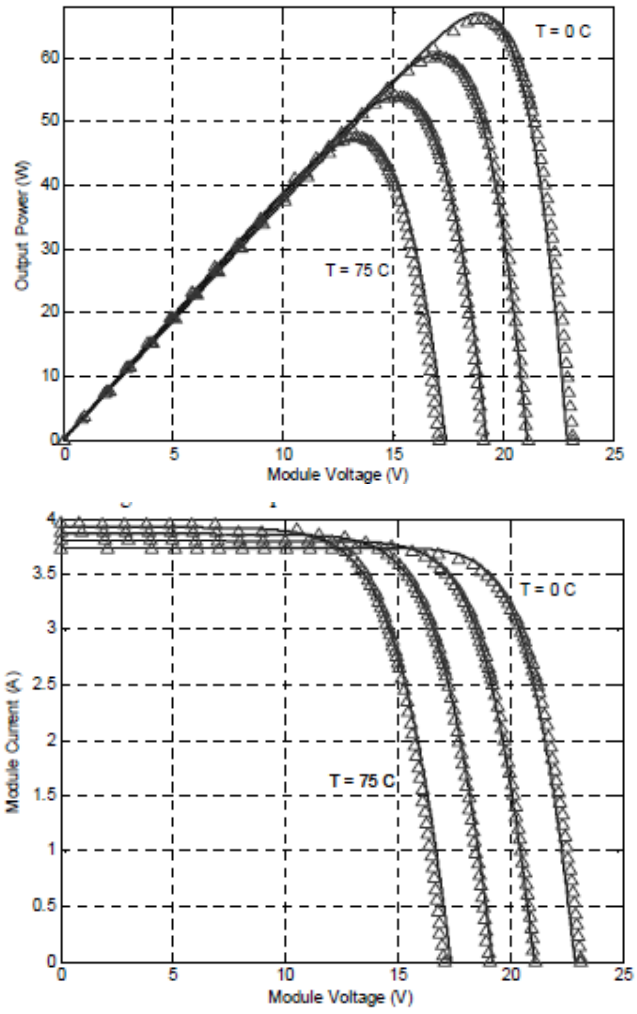

Fig 2.2 Power output and module current Vs voltage at diff temperatures

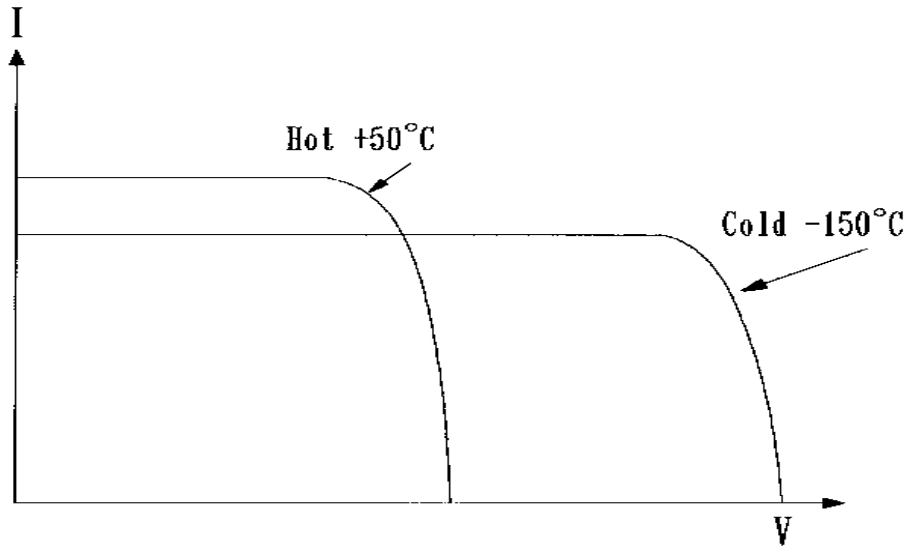

Fig 2.3 Current Vs Voltage at different Temperatures

Effect of temperature on the I-V characteristic. The cell produces less current but greater voltage, with net gain in the power output at cold temperature.

With increasing temperature, the short-circuit current of the cell increases, whereas the open-circuit voltage decreases. The effect of temperature on the power is quantitatively evaluated by examining the effects on the current and the voltage separately. Say I_o and V_o are the short-circuit current and the open-circuit voltage at the reference temperature T, and α and β are their respective temperature coefficients. If the operating temperature is increased by ΔT, then the new current and voltage are given by the following:

$$I_{sc} = I_o (1+ \alpha \cdot \Delta T) \text{ and } V_{oc} = V_o (1- \beta \cdot \Delta T)$$

the new power is as follows:

$$P = V.\ I = I_o (1+ \alpha \cdot \Delta T) * V_o (1- \beta \cdot \Delta T)$$

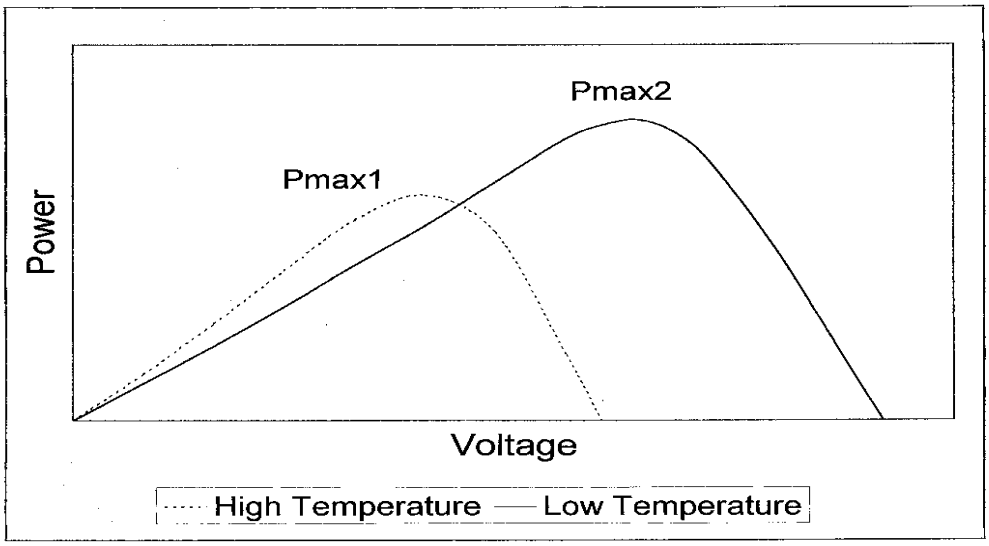

Fig 2.3 Power Vs Voltage at different Temperatures

If the module is to be operated at its maximum there are two possibilities

1. The temperature of the panel should be maintained as close as possible to the standard operating conditions.

2. The panel should be operated as close as possible to the Max. power point using maximum power point tracker.

Out of these two options, even if max. Power point tracker gives the best operating point but the panel is not utilised to its maximum capacity as can be seen from the figure above, The power output of the panel itself decreases as the temperature increases.

For overcoming this drop of power output of the solar panels which are normally operated in the open, sunlight falling on the panel resulting in increase in the temperature of the panel and increase of the ambient temperature, a system is proposed for cooling the solar panels and using the heat thereof for heating the sea water for desalination. Thus the heat which was

causing decreased output of the panel will now be useful, hence increasing the overall efficiency of the system.

2.1.1 MPPT

Maximum power point trackers (MPPTs) are used to track the peak output power of the solar photovoltaic sources. The maximum available power is tracked using specialized algorithms such as Perturb and Observe (P&O), which is an industry standard. The classical P&O algorithm requires the use of both voltage and current sensors. This classical algorithm also requires ad-hoc tuning measures at design time for selecting the right size of the search step. In most cost- and space-constrained systems, an algorithm with minimal sensing It utilizes instantaneous voltage ripples at PV panel output terminals caused by the switching of a chopper connected to the panel in order to identify the direction for the maximum power point (MPP). The tracking for the MPP is achieved by a feedback control of the average terminal voltage of the panel. Appropriate use of the instantaneous and the average values of the PV voltage for the separate purposes enables both the quick transient response and the good convergence with almost no ripples simultaneously.

2.1.2 Battery Energy Storage System (BESS)

The penetration of renewable sources (particularly Solar power) in to the power system network has been increasing in the recent years. As a result of this, there have been serious concerns over reliable and satisfactory operation of the power systems. One of the solutions being proposed to improve the reliability and performance of these systems is to integrate energy storage devices into the power system network. The Deep Cycle batteries used are designed to be discharged and then re-charged hundreds or thousands of times. These batteries are rated in Amp Hours (ah) - usually at 20 hours and 100 hours. Simply stated, amp hours refers to the amount of current - in amps - which can be supplied by the battery over the period of hours. For example, a 350ah battery could supply 17.5 continuous amps over 20 hours or 35 continuous amps for 10 hours. To quickly express the total watts potentially available in a 6 volt 360ah battery; 360ah times the nominal 6 volts equals 2160 watts or 2.16kWh (kilowatt-hours). Like solar panels, batteries are wired in series and/or parallel to increase voltage to the desired level and increase amp hours.

The battery should have sufficient amp hour capacity to supply needed power during the longest expected period "no sun" or extremely cloudy conditions. A lead-acid battery should be sized at least 20% larger than this amount. If there is a source of back-up power, such as a standby generator along with a battery charger, the battery bank does not have to be sized for worst case weather conditions.

The size of the battery bank required will depend on the storage capacity required, the maximum discharge rate, the maximum charge rate, and the minimum temperature at which the batteries will be used. During planning, all of these factors are looked at, and the one requiring the largest capacity will dictate the battery size.

One of the biggest mistakes made by those just starting out is not understanding the relationship between amps and amp-hour requirements of 220 volt AC items versus the effects on their DC low voltage batteries. For example, say you have a 24 volt nominal system and an inverter powering a load of 3 amps, 220VAC, which has a duty cycle of 4 hours per day. You would have a 12 amp hour load (3A X 4 hrs=12 ah). However, in order to determine the true drain on your batteries you have to divide your nominal battery voltage (24v) into the voltage of the load (220v), which is **9**, and then multiply this times your 220vac amp hours (**9** x **12 ah**). So in this case the calculation would be **110 amp hours** drained from your batteries - not the 12 ah. Another simple way is to take the total **watt-hours** of your 220VAC device and divide by nominal system voltage. Using the above example; 3 amps x 220 volts x 4 hours = 1440 watt-hours divided by 24 DC volts = 110 amp hours.

Lead-acid batteries are the most common in PV systems because their initial cost is lower and because they are readily available nearly everywhere in the world. There are many different sizes and designs of lead-acid batteries, but the most important designation is that they are deep cycle batteries. Lead-acid batteries are available in both wet-cell (requires maintenance) and sealed no-maintenance versions. AGM and Gel-cell deep-cycle batteries are also popular because they are maintenance free and they last a lot longer.

2.1.3 Controls and power conditioning system (C-PCS)

The C-PCS form a vital part of the BESS. It interfaces the batteries to the loads (utility/end user) and regulates the battery charge/discharge, charging rate, etc. The C-PCS cost is

significant and it can be greater than 25% of the overall energy storage system. However, this technology is maturing rapidly due to the recent developments in the power conditioning systems of the renewable and distributed energy sources. At present research is being carried out to reduce the overall cost, improve reliability, and develop more efficient and better packaging of power conditioning system.

BESS controls designed for improving power system reliability and power quality (direct power system application)

The enormous development in designing the BESS controls can be attributed to a large extent to the rapid growth in power electronic devices. The BESS controls designed for direct power system applications either consider interconnected system or isolated systems or hybrid systems.

2.1.4 Literature survey for Modeling

Equations for the VI characteristics equation of a PV cell, and Equation expresses an empirical formula of saturation current. Simulated result has been compared with the real output data of the established PV panel.**[1]** As a result, two values were very matched. A novel MPPT control meth!od called the reference voltage control has been proposed, and simulated of the PV generation system including the MPPT control using the DC-DC converter. Consequently, the reference voltage control was stable and more efficient control method comparison with the power comparison MPPT control. So, the validity of the proposed control method has been examined. The details of module costs and efficiency are the most important determining factors for any technology. The two most influential elements in the equation determining the cost of solar photovoltaic electricity are the price per peak Watt of PV modules, and the conversion efficiency of modules, expressed in W/m2.**[2]** The first is generally the dominant factor in the overall installed cost of systems, and it has been steadily declining for the past twenty-five years. New crystalline PV technologies that improve efficiency, among other things, eliminate the need for front-side metal grid lines and are achieving efficiencies approaching 20% on flat plate (non-concentrator) modules. Technologies that combine multiple layers of PV to absorb various portions of the spectrum also increase efficiency. As one example of a highly efficient product, Sanyo's HIT approach (this stands for *H*etero junction

with *I*ntrinsic *T*hin Layer) combines a crystalline PV cell with a thin Amorphous PV layer to achieve roughly a 16.1% module efficiency. The latest efficiency in inverter technology, The dc to ac conversion efficiency of nearly all modern inverter units exceeds 90% and many exceed even 95% at peak load. A hybrid control strategy for photovoltaic (PV) simulator, which emulates the output characteristics of PV arrays under different irradiation, temperature, and loads. The mathematic modeling of the I-V curve of PV arrays when investigated and accordingly the voltage control or current control method is worked out for different segments of PV output characteristics. The hybrid control strategy divides the I-V characteristics of PV arrays into three segments, by measuring the output voltage and current of the PV simulator, the control unit calculates and controls the voltage or current respectively. **[3]** A 2-kW prototype has been built and tested with a variable resistive load and a constant power load as well. Experiment results show that the PV simulator could shift smoothly on its I-V characteristics, which fits well for further experiments of inverters and the maximum power point tracking in the PV system. Algorithms for improving the maximum power point tracking (MPPT) in photovoltaic (PV) systems improves tracking speed and stability, and addresses the problems of unstable atmospheric conditions and partial shading. It incorporates a new adaptive step size, based on detailed analysis of power as a function of duty cycle. The algorithm invokes (i) an online current measurement to improve the dynamic response and (ii) periodic interrupts for detection of partial shading. **[8]**The proposed algorithm is modeled in *Simulink* with a buck converter and simulation results validating its performance and robustness are verified.

2.2 Constant Parameter Theory of Themoelectric generation

In order to set the framework for the numerical method some of the basic thermoelectric equations derived from the simplifying assumptions made over 30 years ago are reviewed. The heat balance at the cold junction of a thermoelectric pellet (hereafter referred to as a pellet) is given by:

$$Qc = \alpha I\, T_c - \boldsymbol{I^2R/2 - K(T_h - T,)}$$

where Q_c is the heat pumped at the cold junction, α is the Seebeck coefficient, I the electrical current, T_c the cold junction temperature, R the electrical resistance, K the thermal conductance and T_h the hot junction temperature. The voltage across this pellet is given by:

$$V = \alpha(T_h - T_c) + IR$$

The heat rejected by the hot side of the pellet, Q_h, is equal to the sum of Q_c plus the power consumed, IV. This yields the following expression for T_c:

$$T_c = T_h - (\alpha I T_c - I^2R/2 - Q_h)/K$$

These "closed-form" or "analytical" equations were derived by applying the simplifying assumption that the thermoelectric parameters α, R, and K were invariant with temperature. This assumption only holds for very small $(T_h - T_c)$ differentials. The most essential input to an accurate thermal model for a pellet is the temperature-dependent thermoelectric material parameters: Seebeck coefficient, electrical resistivity, thermal conductivity, and figure-of-merit.

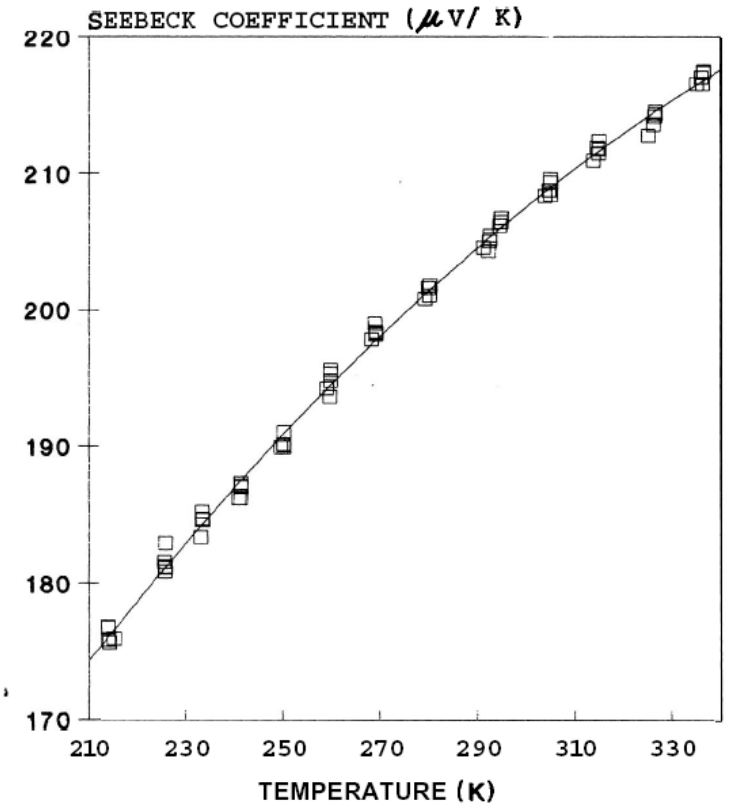

Fig 2.4 Seebeck coefficient test data

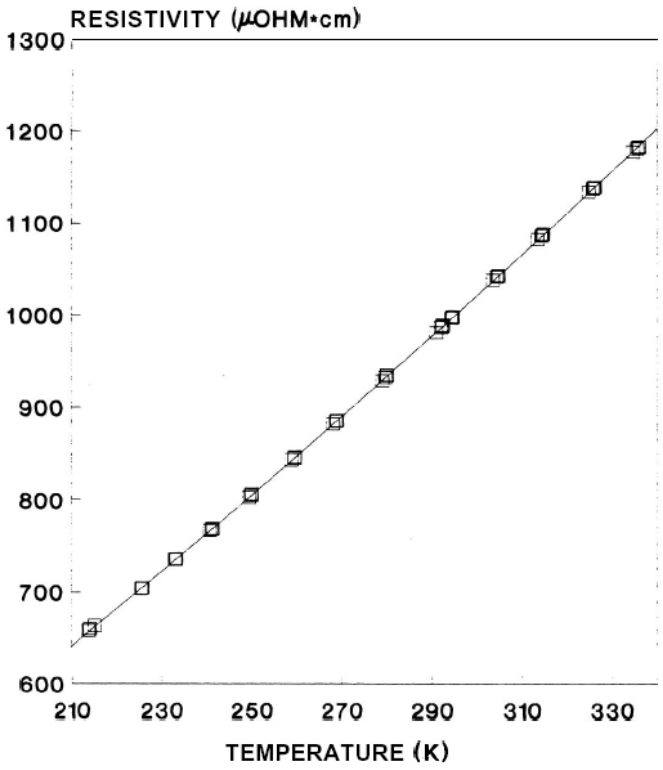

Fig 2.5 Electrical resistivity test data

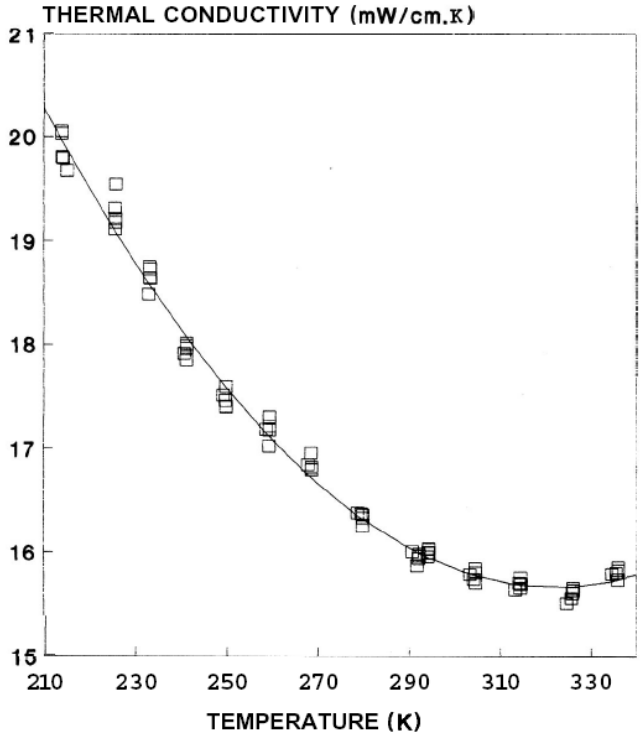

Fig 2.6 Thermal conductivity test data

System analysis

A normal thermoelectric generator with a load resistance R_L connected is composed of many thermoelectric elements, which is shown in Fig. 2.7. Each element is composed of Ptype and N-type semiconductor legs, which work between high and low temperature heat reservoirs of which temperature is T_H and T_L respectively. Q_H and Q_L in Fig.2.7 present the heat generator absorbs from high temperature reservoir and the heat it releases to low temperature reservoir per unit time respectively, that is the heat flux between generator and two heat reservoirs.Due to Peltier effect, the heat flux every thermoelectric element of the generator (one pair of P- and N-type semiconductor legs) absorbs from high temperature reservoir (Q_1) and releases to low temperature reservoir (Q_2) are as follows

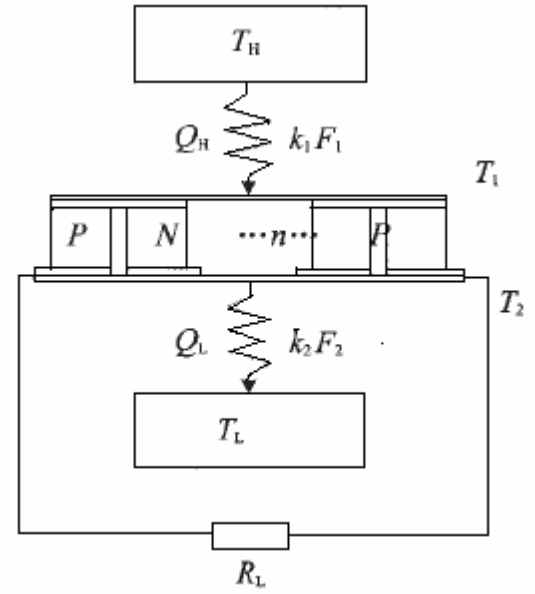

Fig. 2.7 Schematic diagram of multi-element thermoelectric generator

$$Q_1=\alpha I T_1, \tag{2.1}$$

$$Q_2=\alpha I T_2 \tag{2.2}$$

where, I is electric current in generator circuit, T_1 and T_2 are hot-side and cold-side temperature of the generator respectively, $\alpha=\alpha_p-\alpha_n$, while α_p and α_n are the Seebeck coefficients of the P- and N-type semiconductor legs**[10]**. Joulean heat flux one pair of semiconductor legs generates when current goes through is

$$Q_j = I^2 R. \tag{2.3}$$

where

$$R = l_p/(\sigma_p A_p) + l_n/(\sigma_n A_n), \tag{2.4}$$

is the electric resistance of semiconductor couple while l_p, σ_p, A_p and l_n, σ_n, A_n are length, conductivity and cross sectional area of P-type and N-type legs respectively. In order to facilitate the calculation, thermoelectric element is assumed to be insulated thermally, from its surroundings, except at the junction reservoir contacts. There is a heat flux, generated by the temperature difference between both ends of the thermoelectric element according to Newton' law of heat transfer,

$$Q_k = K(T_1 - T_2), \tag{2.5}$$

goes through internal component from hot-side to cold-side,where,

$$K = \lambda_p A_p/l_p + \lambda_n A_n/l_n, \tag{2.6}$$

is thermal conductance of the semiconductor couple (W/K), while λ_P and λ_N are thermal conductivity of P- and N-type legs respectively. Because there is a heat resistance between reservoirs and generator, heat exchange rate is limited, that is a finite time heat transfer. Similarly, employed Newton's law of heat transfer and results above, Q_H and Q_L could be expressed respectively as follows

$$\begin{aligned} Q_H &= k_1 F_1(T_H - T_1) = n(Q_1 + Q_K - 0.5 Q_J) \\ &= n[\alpha I T_1 + K(T_1 - T_2) - 0.5 I^2 R] \end{aligned} \tag{2.7}$$

$$\begin{aligned} Q_L &= k_2 F_2(T_2 - T_L) = n(Q_2 + Q_K + 0.5 Q_J) \\ &= n[\alpha I T_2 + K(T_1 - T_2) + 0.5 I^2 R] \end{aligned} \tag{2.8}$$

where, k_1, k_2 are heat transfer coefficients in hot-side and cold-side heat exchangers ($W \cdot m^{-2} \cdot K^{-1}$), F_1, F_2 are heat transfer surface areas in hot-side and cold-side heat exchangers, n is number of the thermoelectric elements. Temperature difference between the two reservoirs should be

small, not too big at least, according to our analysis in this situation. So, the influence of Thomson effect could be ignored .

$$P = Q_{H\_} Q_L$$

[9] When a thermoelectric generator (TEG) and its external load circuitry are considered together as a system, the codesign and cooptimization of the electronics and the device are crucial in maximizing the system efficiency. The model of thermoelectric battery accounts for all temperature-dependent characteristics of the thermoelectric materials to include the nonlinear voltage, current, and electrothermal coupled effects.

2.3 Photovoltaic Powered Water Pumping Design

Assuming the local meteorology parameters are known, the process starts with a total daily water requirement (Q_{Dr}, in litres/day). Once this has been established, it is possible to calculate pump rate requirements (Q_P, in litres/hour)[6]. The next requirement is to calculate the Total Dynamic Head (TDH) of the pumping installation. Typical data required include static level, draw-down and discharge head, together with installed pipe diameter, pipe length, and fittings used. Compensation for friction and other losses is then computed and combined with other data to determine the TDH for the design. The next step is to determine compensation for friction losses caused by pipes and fittings. A PVPS piping installation consists of lengths of straight pipe, bends, elbows, tees, valves and various other flow impediments, each requiring consideration in the calculation of TDH.

A number of empirical formulae have been developed to solve problems involving pressure drop and friction losses in pipes.

$$H_{FL} = Q_{Pm}^{1.852} (67.03455)/(C_{Hw}^{1.852} - d_i^{4.8655})$$

Where, H_{FL} = Friction head loss (metres per metre of installed pipe)

Q_{Pm} = Volume flow rate (litres per min; = Qp/60)

C_{Hw} = Hazen-Williams Roughness Coefficient

d_i = Installed pipe inner diameter (millimetres)

Now, Total Dynamic Head (TDH) = $L_v + \lambda_{FF} + P_{comp}$

L_v = Total vertical lift

λ_{FF} = Total friction losses (equivalent pipe length, in metres)

P_{comp} = Tank Pressurisation Compensation (metres of head)

$E_{hyd} = Q_{Dr} * TDH/366.972$

Where E_{hyd} = Hydraulic energy required for the project (Wh/day)

The next step in the calculation process is to select a suitable motor/pump and calculate its relative efficiency according to .

$P_{pump} = E_{hyd} / \eta_{pump} * 10$

η_{pump} = Pump efficiency

P_{pump} is Rated Pump Power (Watts)

(This formula assumes an integrated motor/pump combination)

PV array energy (E_{Array}, in Wh/day) and

system load (S_{Load}, in Ah/day),

$E_{Array} = E_{hyd} / \eta_{pump}$

$S_{Load} = E_{Array} * F_{inv} / V_N$

V_N = Nominal System voltage

F_{inv} inverter and control circuitry loss fraction

Preliminary design current (Ampere) , $I_D = S_{Load} / H_T$

Where H_T is Mean monthly irradiation per day ($kWh/m^2/day$)

We can select an appropriate PV module. Data required for module evaluation include material type, short circuit current (I_{SC}), open circuit voltage (V_{OC}), maximum power point current (I_{MP}), voltage (V_{MP}) and power (P_{MP}), nominal operating cell temperature (NOCT).

An array can be characterised by its average efficiency (η_p), which is a function of average module temperature (Tc):

$\eta_p = \eta_r\ [\ 1- \beta\ (T_c - T_r)]/100$

η_r = is the PV module efficiency at reference temperature

T_r (= 25 degrees Celsius), and β is the temperature coefficient for module efficiency (in percent per degree Celsius).

T_c is related to the mean monthly ambient temperature

[4] Vector Control is used to drive the AC motor. This control is done with only two direct measures: two phase input currents. Use of standard asynchronous motors presents lower costs than other commercial systems. The PV array is arranged to cover the possible applications of the Power Conditioner: Pumping, Isolated Home and Multi-point generation. The inverter's tasks are the following:

I.-Extracting the maximum power from the PV array

2.-Feeding the load; controlling flux and speed of the AC machine.

[5] The methods of control and sizing of photovoltaic systems in stand alone PV pumping plants is based on the dynamic model of the PV- DC/DC - Inverter-Asynchronous motor. The DC-DC converter insures an impedance adaptation between the PV and the load and an optimal PV panel output power extraction. However the DC/AC converter insures a PWM control of the induction motor and a sinususoidal output signal. This methodology allows an optimal control and monitoring of continuous-continuous and continuous alternative converters by calculating respectively the DC/DC cyclic ratio and the DC/AC frequency. Contrarily to classic methods, this method which is based on the parametric model of the PV system, leads to a best prediction of the the PV installation especially with load and climatic fluctuations. **[7]** Strategy of modeling and control of photovoltaic pumping systems under MATLAB/SIMULINK

environment. This approach is based on the dynamic model of the "PV- MPPT adapter - Inverter - Asynchronous motor – Pump". The MPPT control allows the extraction of the maximum output power delivered by the PV generator. However the inverter insures a PWM control of the asynchronous motor and a sine waveform of output signals. This methodology allows an optimal control and monitoring of continuous and continuous-alternative inverters by calculating the cyclic ratio of the DC-DC converter and the voltage/frequency (V/f) control law of the DC-DC inverter. This method leads to a best prediction of the behavior and performances of the photovoltaic plant especially in the case of climatic and load fluctuations

2.3.1 Vector control

DC machine like performance can be achieved in induction motor if the machine control is considered in a synchronously rotating reference frame ($d^e - q^e$) where the sinusoidal variables appear as DC quantities in steady state. In figure , the induction motor with the inverter and vector control in the front end is shown with two control current inputs i_{ds}^* *and* i_{qs}^*. These currents are the direct axis component and quadrature axis component of the stator current, respectively, in a synchronously rotating reference frame.

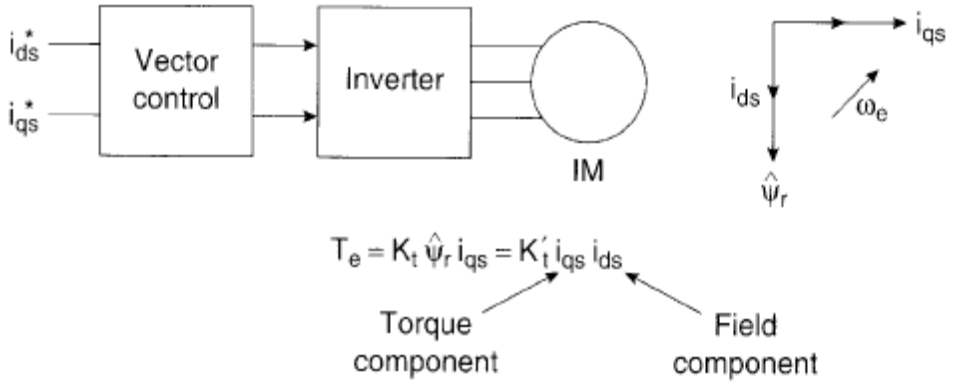

Fig 2.8 : Vector controlled induction motor

With vector control i_{ds} is analogous to field current I_f *and* i_{qs} is analogous to armature current I_a of a DC machine. Therefore, the torque can be expressed as

$$T_e = K_t \psi_r i_{qs} \qquad (1)$$

$$T_e = K_t' i_{ds} i_{qs} \qquad (2)$$

where ψ_r is the peak value of sinusoidal space vector..

The fundamentals of vector control implementation can be explained with the help of Fig 2.9.

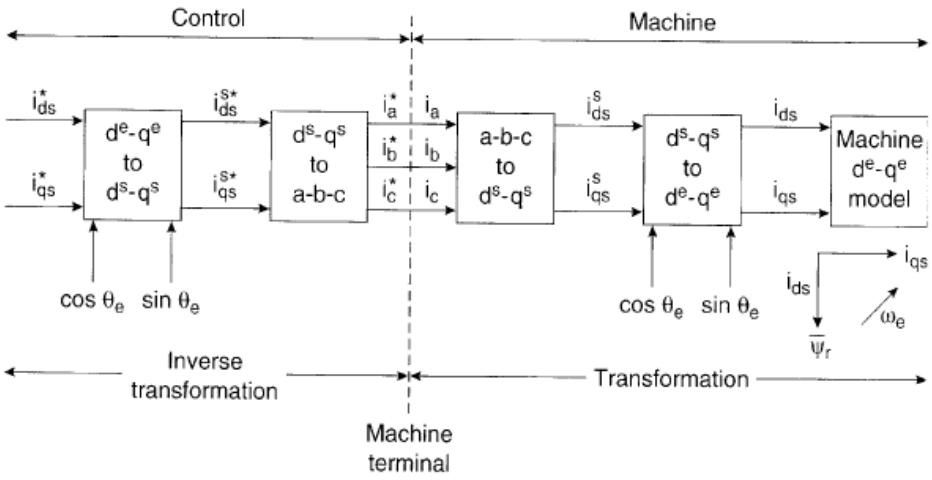

Fig 2.9 vector control implementation principle with machine $d^e - q^e$ model

where the machine model is represented in a synchronously rotating reference frame. The inverter generates currents i_a , i_b , i_c *are* converted to i_{ds}^* *and* i_{qs}^* components by 3φ / 2φ transformation. These are then converted to synchronously rotating frame by the unit vector components cos θ_e and sin θ_e before applying them to $d^e - q^e$ machine model.

Chapter-3

Modeling of components using MATLAB/ Simulink

3.1 General

This chapter deals with modeling of various components viz, PV array, TEG and vector control of AC motor for pump applications. The dynamic model of the system components are developed in MATLAB/SIMULINK and are simulated under dynamic loading conditions. The system performance is also observed under these conditions

3.2 Modelling and Simulation of PV Array

A photovoltaic PV generator is the whole assembly of solar cells, connections, protective parts, supports etc. In the present modelling, the focus is only on cell/module/array. Solar cells consist of a p-n junction fabricated in a thin wafer or layer of semiconductor (usually silicon). In the dark, the I-V output characteristic of a solar cell has an exponential characteristic similar to that of a diode. When solar energy (photons) hits the solar cell, with energy greater than band gap energy of the semiconductor, electrons are knocked loose from the atoms in the material, creating electron-hole pairs . These carriers are swept apart under the influence of the internal electric fields of the p-n junction and create a current proportional to the incident radiation. When the cell is short circuited, this current flows in the external circuit; when open circuited, this current is shunted internally by the intrinsic p-n junction diode. The characteristics of this diode therefore set the open circuit voltage characteristics of the cell.

3.2.1 Model of the PV cell

The simplest equivalent circuit of a solar cell is a current source in parallel with a diode. The output of the current source is directly proportional to the light falling on the cell (photocurrent *Iph*). During darkness, the solar cell is not an active device; it works as a diode, i.e. a p-n junction. It produces neither a current nor a voltage. However, if it is connected to an external supply (large voltage) it generates a current *ID,* called diode (*D*) current or dark current. The diode determines the I-V characteristics of the cell. An equivalent circuit model with current source diode in parallel with series and shunt resistance depicted the characteristics of the substrate is presented in Fig. 3.1.

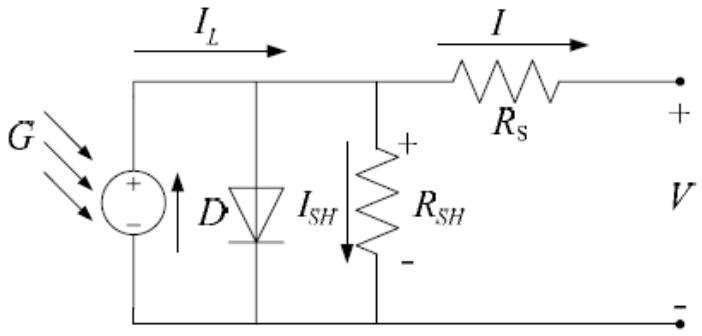

Fig. 3.1 Circuit diagram of the PV model

- Temperature dependence of the diode saturation current I_0.
- Temperature dependence of the photo current I_L.
- Series resistance R_s, which gives a more accurate shape between the maximum power point and the open circuit voltage. This represents the internal losses due to the current flow.
- Shunt resistance R_{sh}, in parallel with the diode, this corresponds to the leakage current to the ground and it is commonly neglected
- Either allowing the diode quality factor n to become a variable parameter (instead of being fixed at either 1 or 2) or introducing two parallel diodes with independently set saturation currents.

In an ideal cell $R_s = R_{sh} = 0$, which is a relatively common assumption. The net current of the cell is the difference of the photocurrent, I_L and the normal diode current I_0 :

$$I = I_L - I_0\left(e^{\frac{q(V+IR_S)}{nkT}} - 1\right) \tag{3.1}$$

The model includes temperature dependence of the photocurrent I_L and the saturation current of the diode I_0.

$$I_L = I_L(T_1) + K_0(T - T_1) \tag{3.2}$$

$$I_L(T_1) = I_{SC}(T_{1,nom})\frac{G}{G(_{nom})} \tag{3.3}$$

$$K_0 = \frac{I_{SC}(T_2) - I_{SC}(T_1)}{(T_2 - T_1)} \tag{3.4}$$

$$I_0 = I_o(T_1) \times \left(\frac{T}{T_1}\right)^{\frac{3}{n}} e^{\frac{qV_q(T_1)}{nk\left(\frac{1}{T} - \frac{1}{T_1}\right)}} \tag{3.5}$$

$$I_0(T_1) = \frac{I_{SC}(T_1)}{\left(e^{\frac{qV_{OC}(T_1)}{nkT_1}} - 1\right)} \tag{3.6}$$

A series resistance R_s was included; which represents the resistance inside each cell in the connection between cells.

$$R_S = -\frac{dV}{dI_{V_{OC}}} - \frac{1}{X_V} \tag{3.7}$$

$$X_V = I_0(T_1)\frac{q}{nkT_1} e^{\frac{qV_{OC}(T_1)}{nkT_1}} - \frac{1}{X_V} \tag{3.8}$$

The shunt resistance R_{sh} is neglected in the present model. A single shunt diode was used with the diode quality factor set to achieve the best curve match. This model is a simplified version of the two diode model.

3.2.2 Model of PV cell as S-function in MATLAB

Based on the above described equations a model in terms of a function is developed in MATLAB environment to facilitate its use with the SIMULINK platform through S-function approach. The variable '*Suns*' inputs the variable solar insolation and '*TaC*' provide the ambient temperature of the site.

```
function Ia=solar(Va,Suns,TaC)
% Ia = solar (Va,G,T)
% Ia,Va = current and voltage
% G = num of Suns (1 Sun = 1000 W/mˆ2)
% T = Temp Celcius
k = 1.38e-23;              %  Boltzman's constant
q = 1.60e-19;                    % charge of electron
n=1.2;                     % diode quality factor
Vg = 1.12;                       % Voltage  band for crystalline silicon, 1.12eV,
% 1.75 for amorphous silicon.
Ns = 36;                         % Number of quality (diodes)
T1 = 273 + 25;
Voc_T1 = 21.06 /Ns;
                                 % open circuit Voltage  at temperature T1
Isc_T1 = 3.80;
                                 % short circuit current at temperature T1
T2 = 273 + 75;
Voc_T2 = 17.05 /Ns;
                                 % open circuit Voltage  at temperature T2
Isc_T2 = 3.92;
                                 % short circuit current at temperature T2
TaK = 273 + TaC;                 ; Temperature in Kelvin
K0 = (Isc_T2 - Isc_T1)/(T2 - T1);                %
IL_T1 = Isc_T1 * Suns;                           %
IL = IL_T1 + K0*(TaK - T1);                      %
I0_T1=Isc_T1/(exp(q*Voc_T1/(n*k*T1))-1);
I0= I0_T1*(TaK/T1).^(3/n).*exp(-q*Vg/(n*k).*((1./TaK)-(1/T1)));
Xv = I0_T1*q/(n*k*T1) * exp(q*Voc_T1/(n*k*T1));
dVdI_Voc = - 1.15/Ns / 2;                        % dV/dI a Voc per cell
Rs = - dVdI_Voc - 1/Xv;                          % Rs series resistance per cell
Vt_Ta = A * k * TaK / q;                         % = A * kT/q
Vc = Va/Ns;
Ia = zeros(size(Vc));                            % Newton
for j=1:5;
Ia = Ia - (IL - Ia - I0.*( exp((Vc+Ia.*Rs)./Vt_Ta) -1))./...
...(-1 - (I0.*( exp((Vc+Ia.*Rs)./Vt_Ta) -1)).*Rs./Vt_Ta);
End
```

The advantage of using the above model lies in variable environmental conditions which are taken care in this model such as temperature dependence of solar cell, effect of solar insolation,

series internal resistance etc. A model of solar cell is also been provided in the SimElectronics blockset of new version of MATLAB / Simulink 2008. Although the model doesn't have the temperature dependence and other environment conditions, but the system cell has been exactly modelled as small signal model matching the test conditions at 25°C. For meeting the dynamic performance of the system the model available in SimElectronics blockset is used for further investigations.

3.2.3 Model of PV in Simulink / Sim electronics

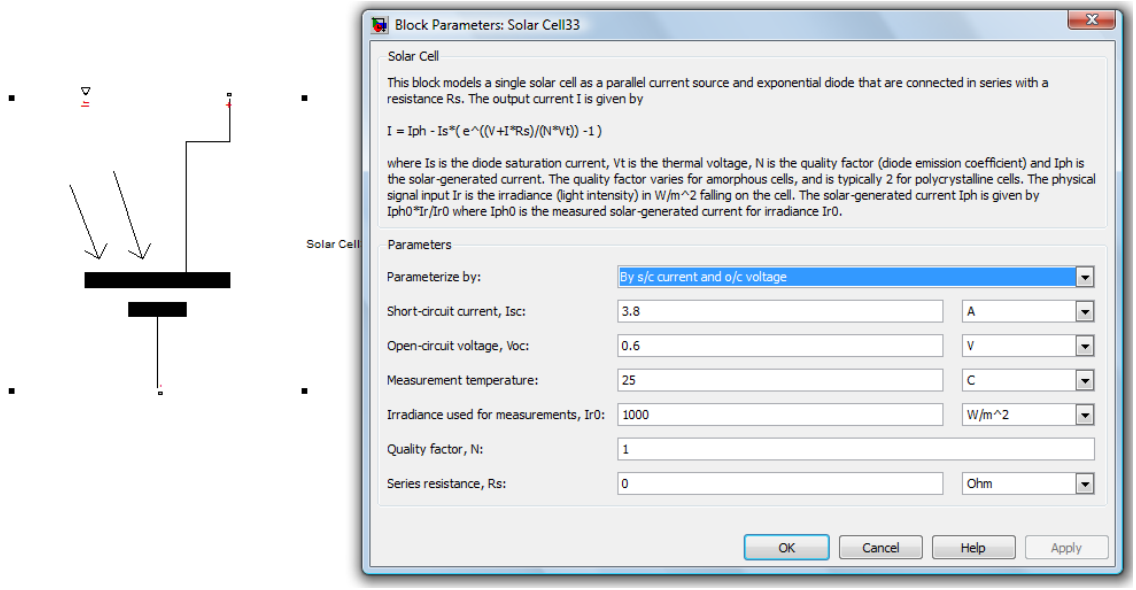

Fig 3.2: Block parameters of solar cell

In the block provided in Sim-Electronics blockset various parameters of the solar cell can be adjusted as shown in the Fig.3.7. In the model short circuit current of the cell can be pre defined, open circuit voltage of the cell can be adjusted according to need and system conditions, base temperature or the measurement temperature at which cell is to be operated can also be provided. The model also allows to select irradiance used for measurement together with quality factor of the diode and internal series resistance R_s .

3.2.4 MATLAB Simulation of PV array

A Solar array is constructed with the help of 32 solar cells in series. The array so formed is depicted in the Fig. 3.6. The expected open circuit voltage has been configured for 19.2 V which on simulation matched the configured value. The individual open circuit voltage of each cell is taken to be 0.6 V. The solar insolation is kept at 1000 W/m^2 which is as per Indian conditions. The short circuit current is selected as 3.8A for the cell / array.

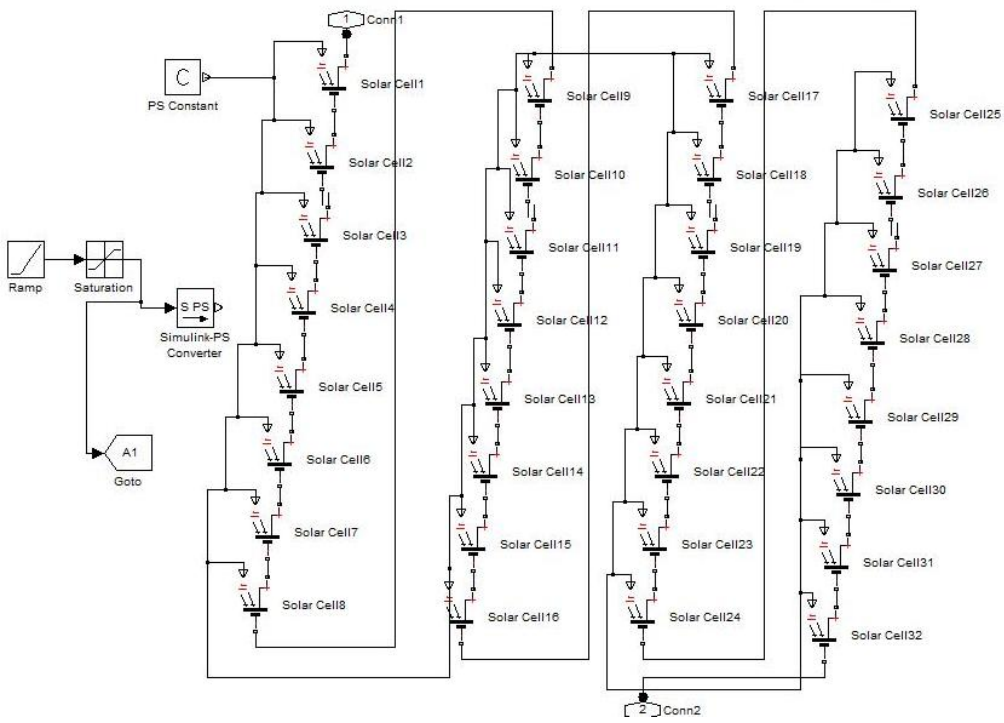

Fig 3.3: PV array showing 32 solar cells connected in series

Performance Evaluation of the PV array

The performance of the PV array has been evaluated through simulation in MATLAB-Simulink environment for the dynamic variations in solar insolation and connected load. The solar insolation is varied between 0 to 1500 W/m^2 to represent the variation experienced from day break till the afternoon when it is maximum. A fixed load resistance is connected across this panel and current and voltage measured. Fig.3.4 depicts the MATLAB-Simulink model of the integrated system. The insolation is varied through a ramp function. The performance of the modeled system is shown in Fig. 3.5. It may be evident from the Fig. 3.5 that when solar insolation increases from dark, ie, zero value to 1W/m^2 the voltage across the panel at once jumps to 15 V and slowly increases with insolation to saturate at 19.2 V at an insolation of 1000 W/m^2. Since the load connected is small and constant the variation of current is not visible in the Fig. 3.5.

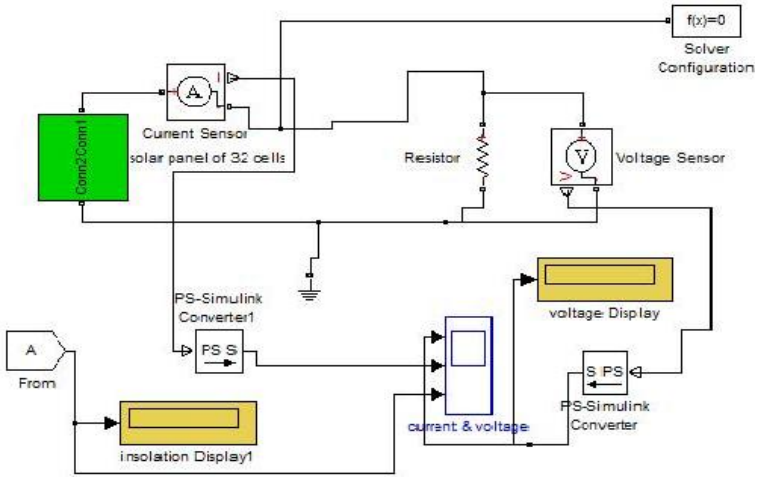

Fig 3.4 Simulation of PV Panel at varying insolation.

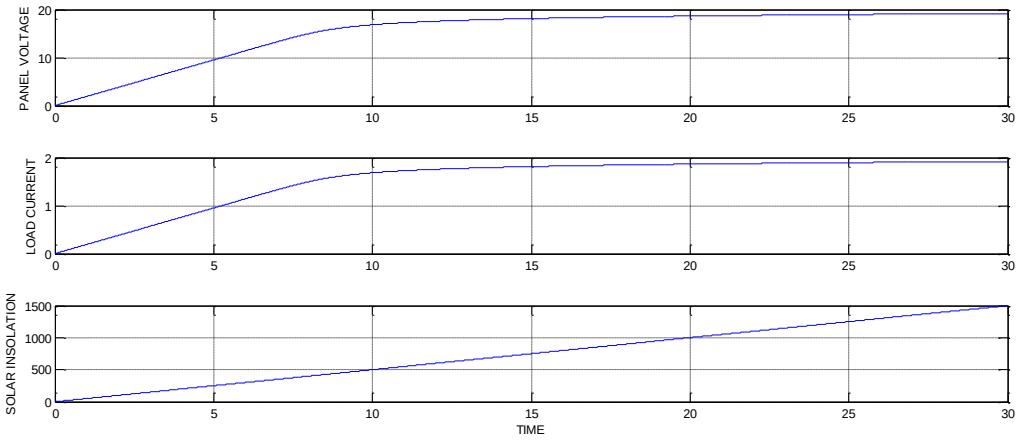

Fig 3.5: Panel voltage and current with varying solar insolation

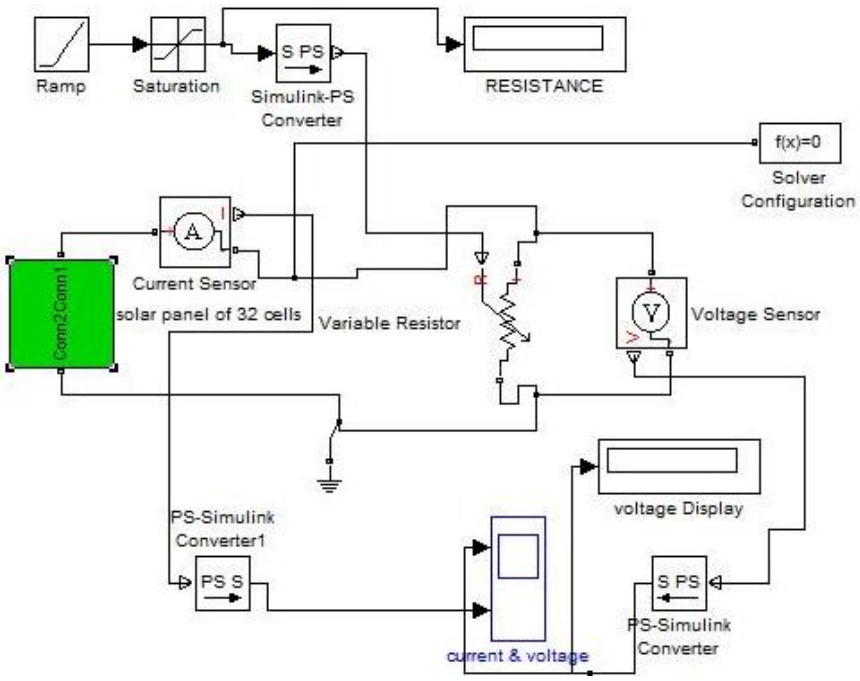

Fig 3.6: Testing of simulated solar panel with varying load

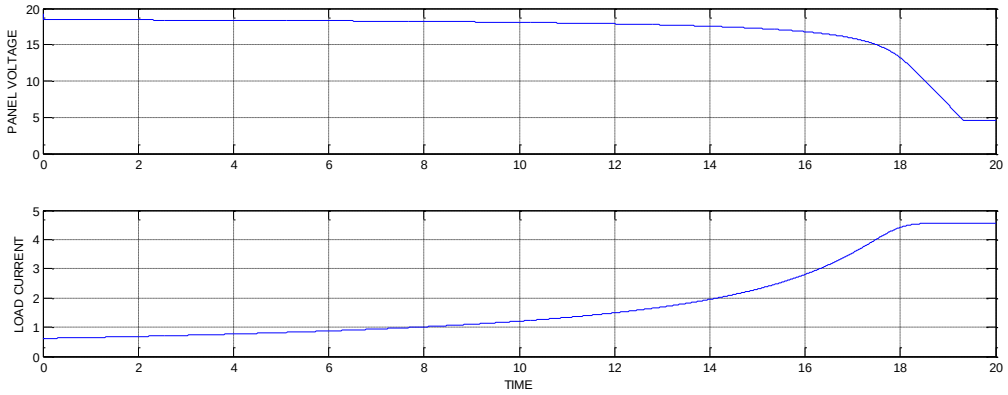

Fig 3.7: Current and Voltage characteristics of PV with varying load

The performance of the PV array for varying load is shown in Fig 3.7 .The same Solar array is used and a varying load is connected across the array. The Load is varied through a ramp function. A current sensor is connected in series with the array. Array is kept at a fixed solar insolation i.e. 1000w/m^2 which is average value of solar insolation in Indian conditions. The performance of the modeled system is shown in Fig. 3.7. When the load is increased i.e. resistance is decreased, The current of the array increase slowly without affecting the voltage output but as the current increases close to short circuit value the voltage abruptly starts decreasing and becomes zero as the current increases further. The knee point at which the voltage starts decreasing is actually the maximum power point of the array. It is evident from the performance curve that the array must be operated near to the maximum power point (MPP) so that maximum power can be drawn from a given array, further if MPP is crossed by way of connecting excess load, the voltage of the array does not remain constant and dips abruptly which is visible clearly in Fig 3.7.

3.2 TEG Simulation

$P = n [\alpha^2(T_1-T_2)^2 * R_L] / (R+R_L)^2$

Power output of the thermoelectric module depending on the

Temperatures T_1 & T_2 of the surfaces of the generator

n = no of thermoelectric elements

α = $2.3 \text{ X } 10^{-4}$

$T_1 = 150^oC$

$T_2 = 50^oC$

$R = 2.3622 \text{ X } 10^{-4} \Omega$

$R_L = 0.3 \Omega$

Performance Evaluation of the thermoelectric module

Fig 3.8 shows the block diagram of the thermoelectric module which is simulated using MATLAB. Thermoelectric module with 50 pn legs is subjected to a temp difference, one side is kept at 50^0 c and the temperature of other side is increased from 50 to 150^0c using a continuously increasing ramp signal. Fig 3.9 shows the variation of the power output of the module with the change in temperature of the hot side of the thermoelectric generator (TEG). When the temperature difference increases we see that power output curve becomes parabolic. This property of TEG can be used along with PV panel in two ways; one is if TEG is used to generate power using the heat in the PV panel because of direct sun heating and thus utilizing that heat to convert it to power, other way is that TE module is used along with PV panel as coolers which will cool the PV panel and hence the efficiency of the PV panel will increase because of its lower operating temperature.

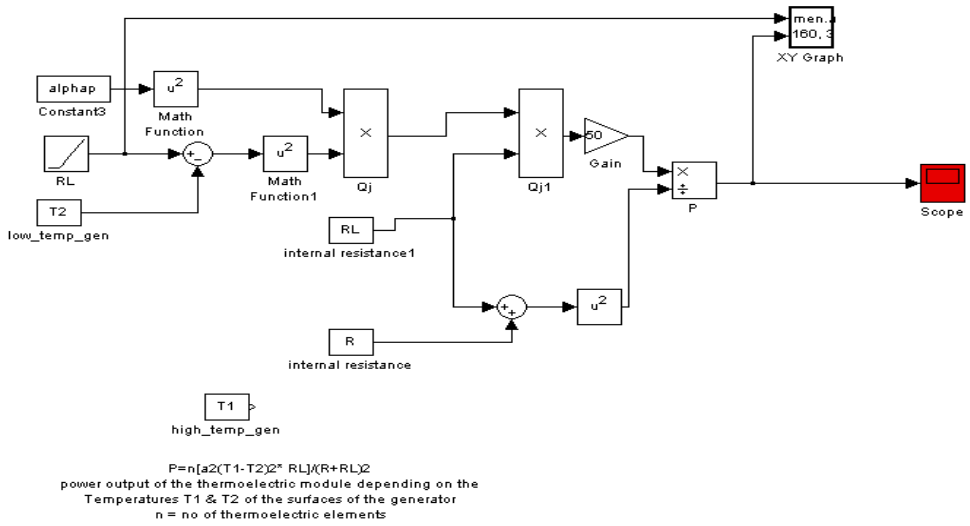

Fig 3.8: Simulation of Thermoelectric module with 50 pn

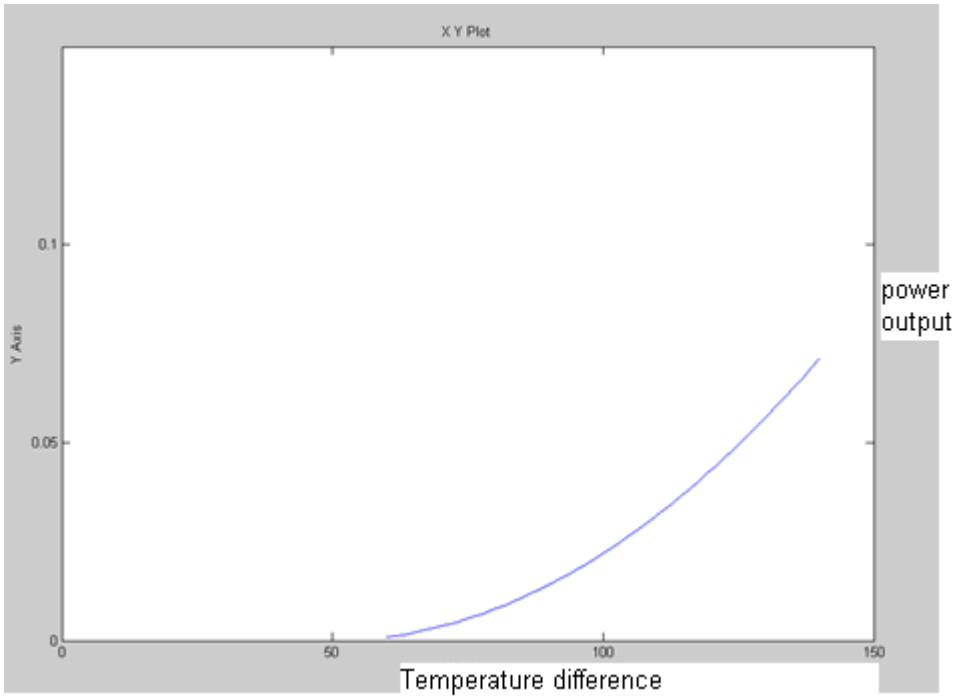

Fig 3.9: power output of the thermoelectric module with 50 pn legs

3.4 Vector Controller for AC motor :

The simulation model have been developed in MATLAB environment along with simulink and power system block set toolbox .

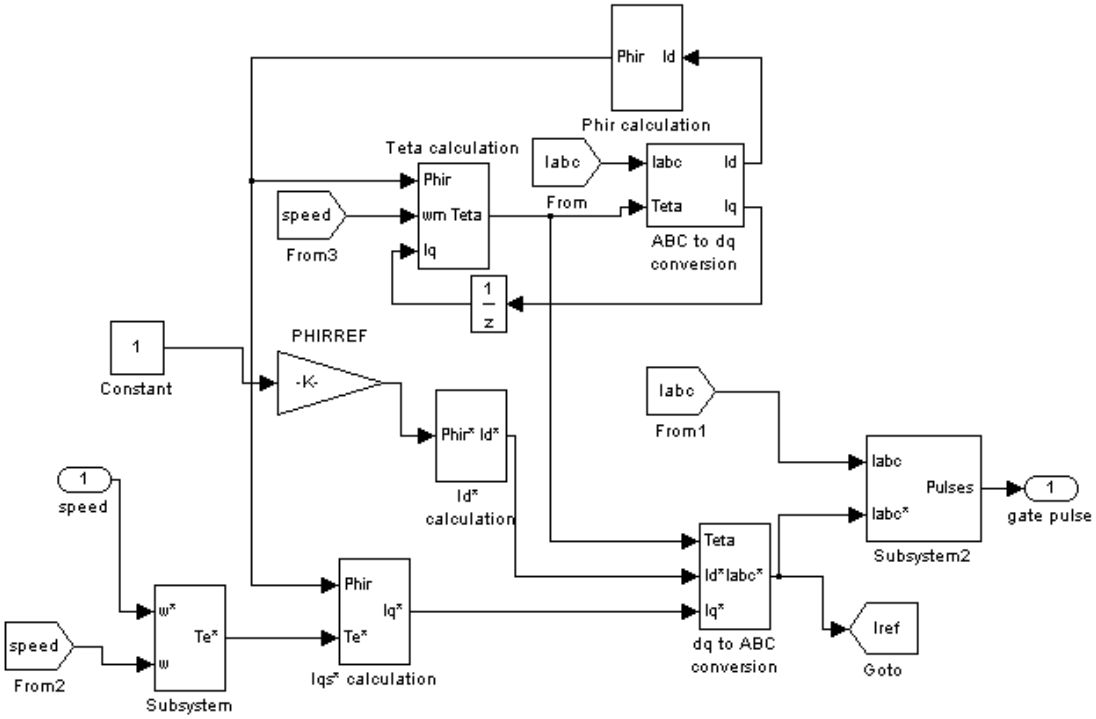

Fig 3.10: Vector Controller designed in simulink for Pump/motor

Speed controller

The model of speed controller has been realized in using simulink tool box of the MATLAB software The main function of speed controller is to provide the reference for the vector controller. The output of speed controller is limited to a proper value in accordance to the motor rating to generate the reference torque for the vector controller. The speed controllers realized using the simulink tool box is PI speed controller.

Fig. 3.10 shows the simulink model diagram of the PI speed controller in discrete frame. The basic operating equation have been stated in subsection

Vector controller

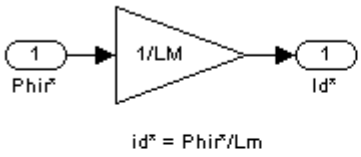

Fig 3.11: Reference flux to ref magnetizing current conversion block

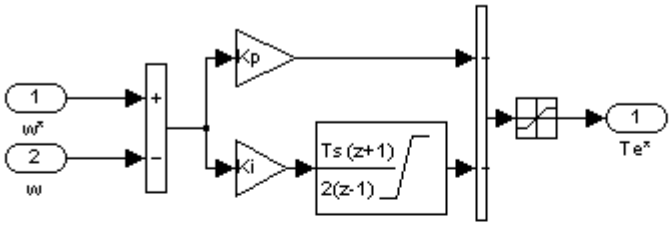

Fig 3.12: Reference Torque generation by comparing speed of motor with ref speed

```
PVA= 746          VLL= 415
F=50              RS=14.98
LLS=0.04          RR=7.74
LLR=0.04          LM=.54
J=0.0018          P=2
TLIM=7            PHIRREF=0.48
Ki =0.0295        Ts=78.125e-6
Kp =0.0895
h=0.2             Cq =7
```

Fig 3.11 shows the calculation of reference flux component of the stator current i_d^* in synchronously rotating reference frame using referencing rotor flux Ψ_r obtained from the no load testing of the motor Fig 3.12 shows calculation of reference torque component of the stator current i_q^* in the synchronous rotating reference frame using the reference torque from the speed controller T^* & Ψ_r

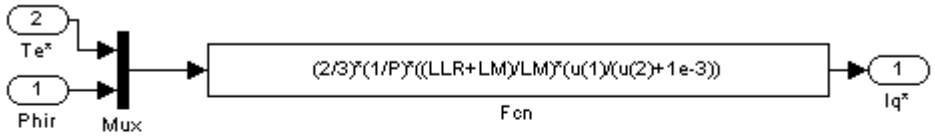

Fig 3.13: Ref i_q generation

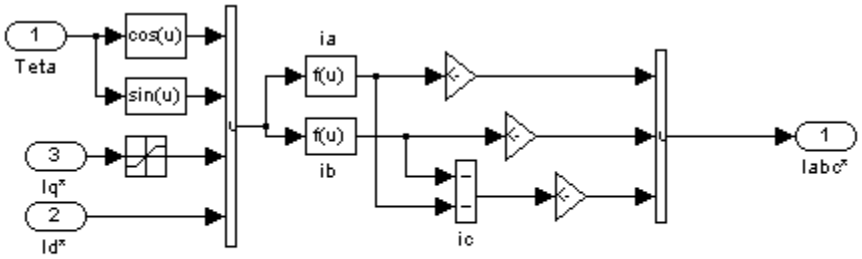

Fig 3.14: 3 Phase ref current generation

Fig 3.14 shows the calculation of reference currents by transformation of d-q components into reference abc components.

Three phase rotating to two phase converter

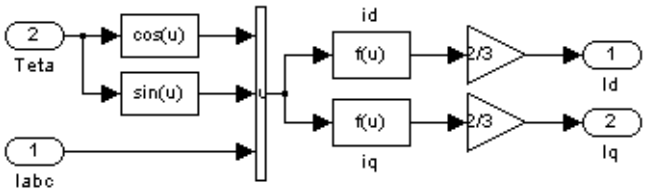

Fig 3.15: Three phase current to 2 vector converter block

This developed subsystem Fig 3.15 using simulink toolbox carries out conversion of the quantities from the three phase synchronously rotating frame to two phase stationary reference frame i_q and i_d for estimating stator flux and theta calculation.

Hysterisis current controller

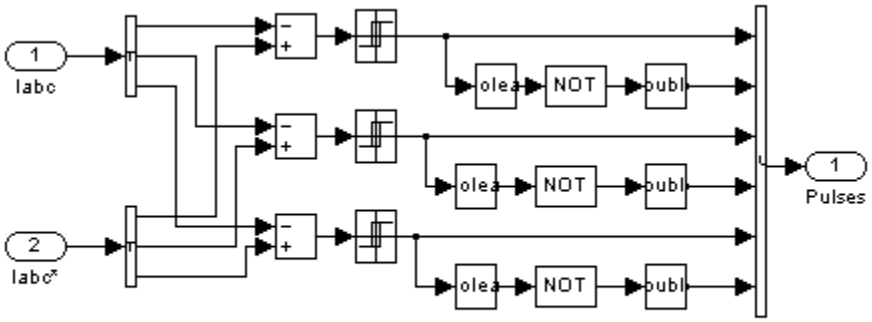

Fig 3.16 : comparison of 3 phase motor with reference current and generation of 6 pulses for three phase power inverter

There are two types of current controllers for voltage fed PWM inverters

1 Hysteresis current controller

2 2 Ramp comparison controller

Fig 3.16 shows the Hysteresis current controller, it does not require system parameters in order to use in controllers. Three phase ref sine waves proportional to the desired currents based on certain criteria are generated and compared with the measured instantaneous values of the output currents. The hysteresis comparator has a dead band that permits a deviation of ΔI of the actual current from the ref wave. If an actual phase current exceeds the current ref by the hysteresis band, the upper devise in the inverter leg of that phase is turned off and the lower device is turned on. This causes the phase current to decay until the current error reaches the lower limit when the switch status is reversed, causing the current to rise again

***Performance evaluation of integrated system*:**

Fig 3.17 shows various components of the whole setup, the power requirement is purely met up from the PV panel which is shown in orange color. This PV panel module is basically a collection of eight PV arrays with cumulative voltage output of 361 V. This PV panel module supplies power to the 3 phase bridge inverter which is controlled by the vector controller. The main function of speed controller is to provide the reference torque for the vector controller. The output of speed controller is limited to a proper value in accordance to the motor rating to

generate the reference torque for the vector controller. The speed controllers realized using the simulink tool box is PI speed controller. Fig. 3.10 shows the simulink model diagram of the PI speed controller in discrete frame. The basic operating equations have been stated in subsection. Fig 3.11 shows the calculation of reference flux component of the stator current i_d^* in synchronously rotating reference frame using referencing rotor flux Ψ_r obtained from the no load testing of the motor Fig 3.12 shows calculation of reference torque component of the stator current i_q^* in the synchronous rotating reference frame using the reference torque from the speed controller T^* & Ψ_r This developed subsystem Fig 3.15 using simulink toolbox carries out conversion of the quantities from the three phase synchronously rotating frame to two phase stationary reference frame i_q and i_d. Fig 3.16 shows the Hysteresis current controller, it does not require system parameters in order to use in controllers. Three phase ref sine waves proportional to the desired currents based on certain criteria are generated and compared with the measured instantaneous values of the output currents. The hysteresis comparator has a dead band that permits a deviation of ΔI of the actual current from the ref wave. If an actual phase current exceeds the current ref by the hysteresis band, the upper devise in the inverter leg of that phase is turned off and the lower device is turned on. This causes the phase current to decay until the current error reaches the lower limit when the switch status is reversed, causing the current to rise again

Starting dynamics

When three phase squirrel cage induction motors are fed from a controlled voltage and frequency source, the motor is started at low frequency decided by the controller and finally runs at the steady state condition at the set reference value of speed. The reference speed here is set at 1430 rpm with a torque limit set as per the pump characteristics. In each case the starting current is also inherently limited within the twice of the rated current. When the motor builds up the required starting torque to reach the set reference speed, the speed error reduces to almost zero rpm the winding current also reduces to the rated value and the developed torque becomes the load torque as observed in the starting response shown in Fig 3.18. The rise time of speed from 0 to 90 % is 0.08 s with no overshooting of speed.

Fig 3.17 :Simulation of PV powered vector controlled pump/motor.

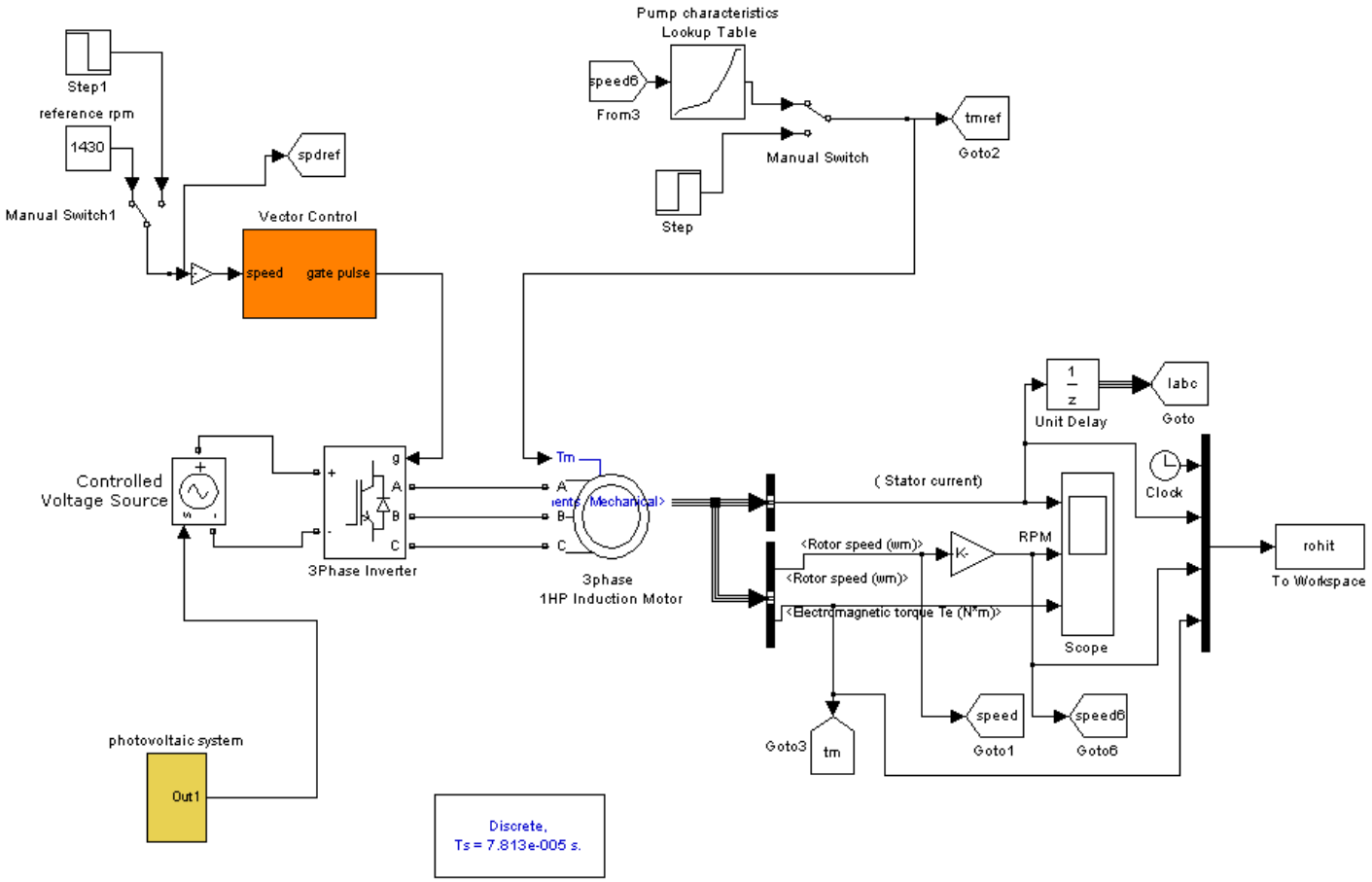

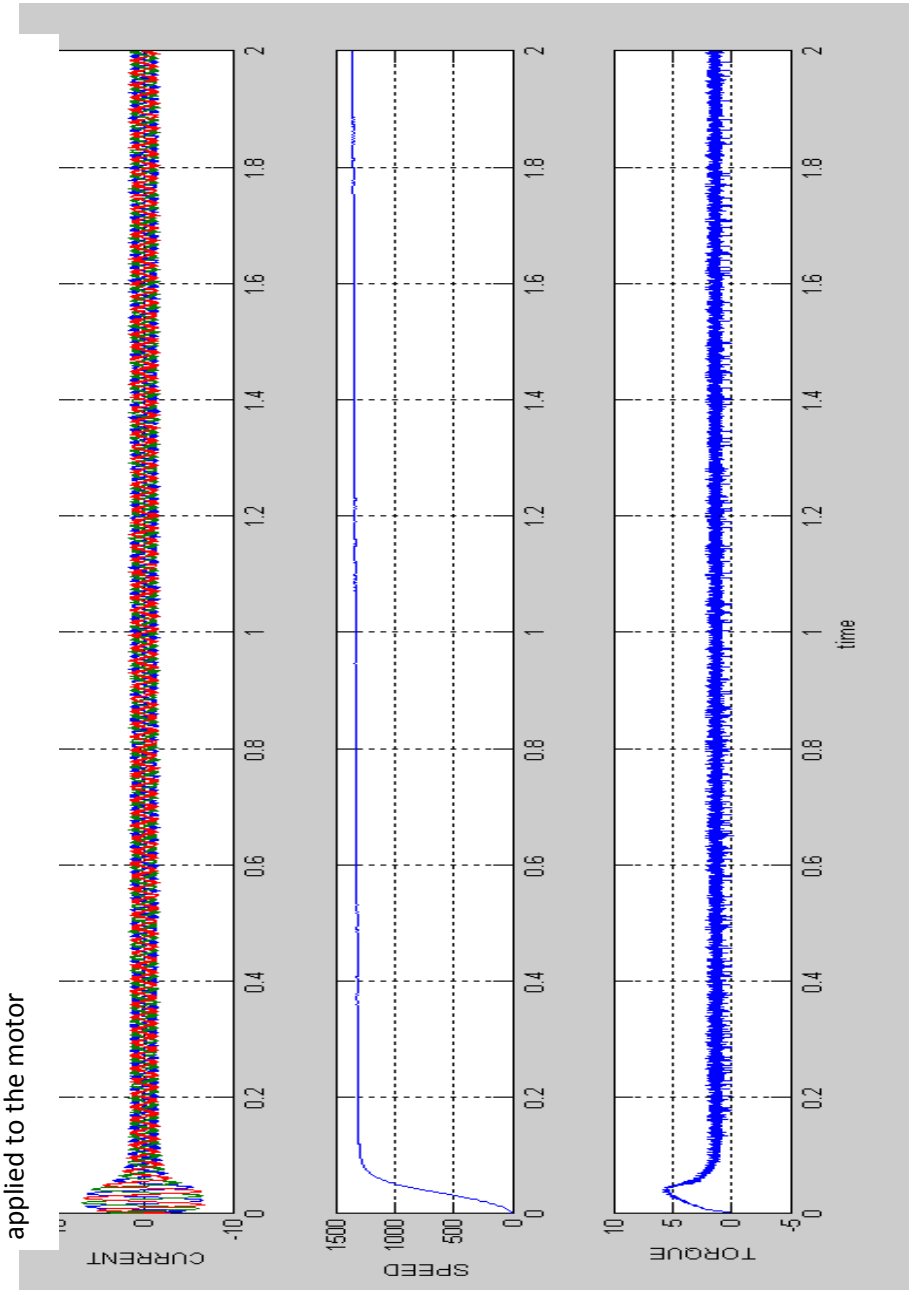

Fig 3.18 : The output graphs show the response of the machine/ controller when pump load is applied to the motor

Load perturbation

As shown in Fig 3.19 when the motor is running at steady state a load torque equal to the rated torque of the motor is applied on its shaft at t = 0.5. Sudden application of load caused an instantaneous drop in speed of the motor. In response to the drop in speed, the output of the speed controller responds by increasing the reference torque T^* value. Therefore the developed electromagnetic torque of the induction motor increases, causing the motor speed to settle to the reference value with the increased winding current. Hence the motor is operating at steady state. On load, if sudden load is removed at t = 1.4 s which causes a small overshoot in the rotor speed because of the small overshoot input become negative and consequently the output of PI controller T^* reduces . Normal control structure results in change in electromagnetic torque developed by the motor. This causes reduction in the rotor speed and hence the speed decreases and settles to the reference values. After the removal of load the load current also reduces.

Fig 3.19 : Current and Speed graphs when load torque is first changed from 0.2 to 1.5 at t=0.5s and then Tis changed from 1.5 to 0.2 .The output shows how the machine settles.

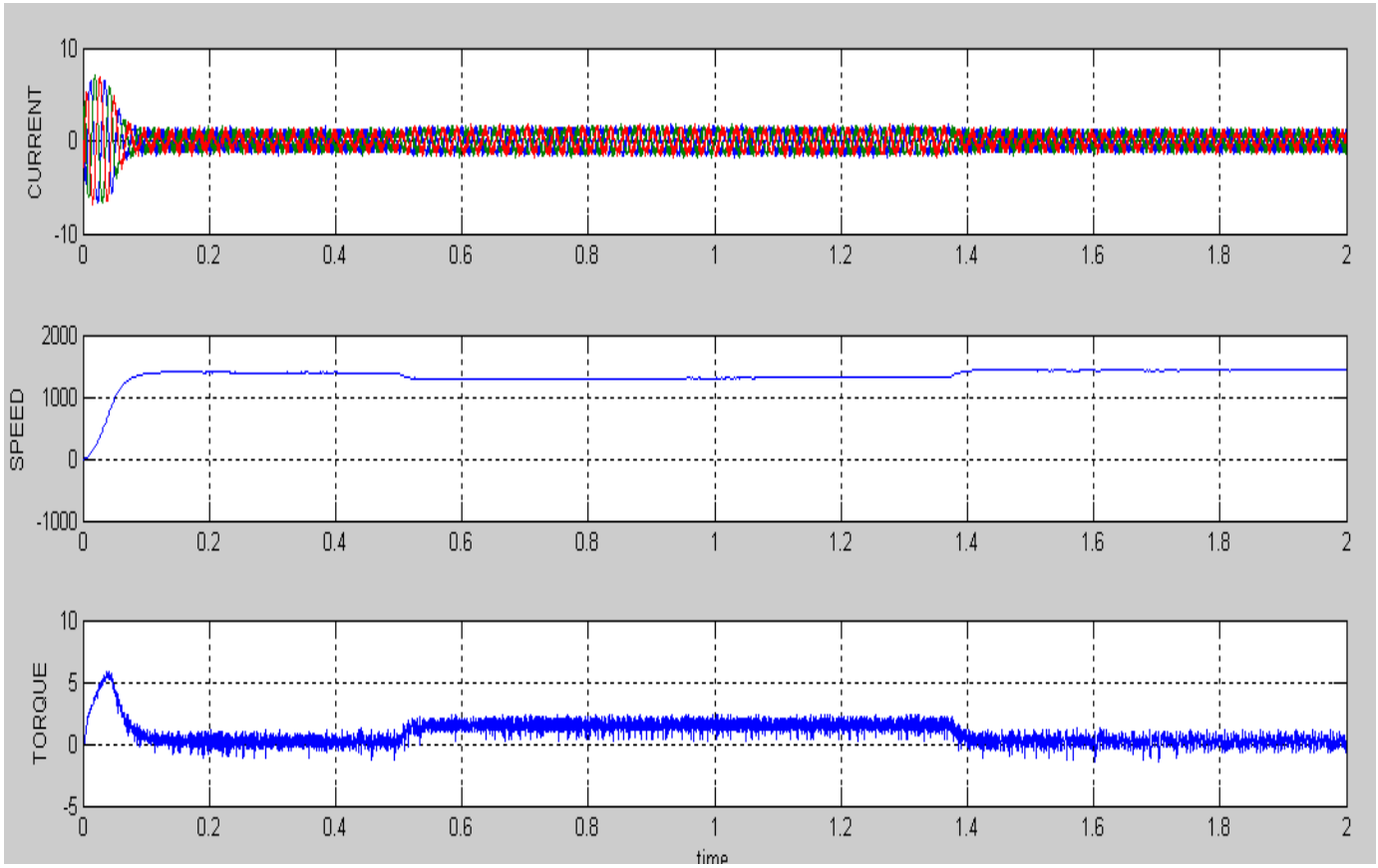

Chapter 4

PV- TE Hybrid Systems

4.1 General

As seen in preceding sections the efficiency of Photovoltaic systems deteriorates with the increase in temperature. However, concentrating the light on PV array surface increases its efficiency but, poses further problem of deterioration due to additional concentration of heat. Though the idea of light concentration to replace expensive solar cell area by optical components like mirrors and lenses suggest cheaper alternatives, but, the fruitfulness can only be achieved when the heat accumulated at the PV array is discharged to ambience without increasing the temperature of the surface. Under such conditions very expensive high-efficiency special crystalline cells of multilayer tandem having efficiencies above 30% can also be used. If conventional passive heat sink is used it will become bulky and slow in dynamics as the level of concentration is increased. For such type of applications active heat sinks such as *Thermoelectric Coolers* can be used. In this chapter a hybrid of PV–TE is proposed which can offer the best choice for concentrating type of systems. The subsequent section of the chapter deals with hybrid PV-TE system for its overall performance improvement.

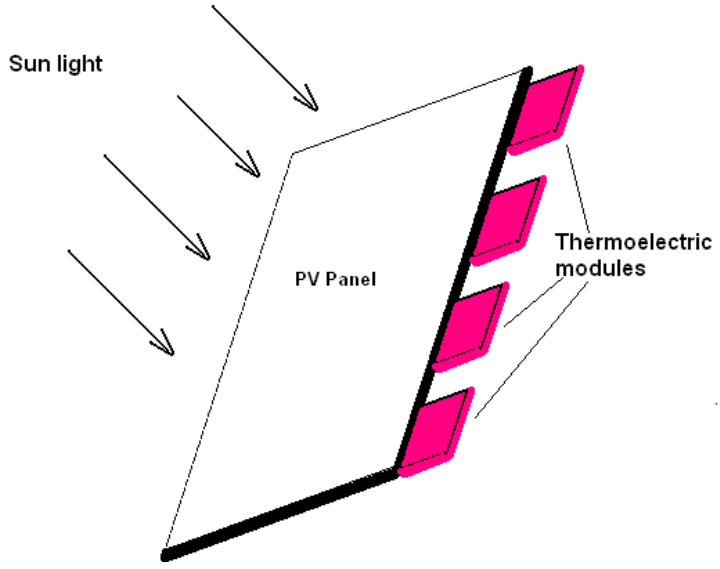

Fig 4.1 : Thermoelectric modules attached on the back of PV Panel

4.2 Hybrid Photovoltaic –Thermoelectric Generator

If PV panel is used in configuration as shown in Fig.4.1, thermoelectric modules are placed on the back of the PV panels which can collect the heat from the PV panel very fast through drawl of current absorbing extra heat with respect to ambience. This way the extra heat will be removed from PV panel and its efficiency would increase, as its operation at 25℃ yields highest efficiency, together with this, the TE system would also produce additional electric power. For instance, the operating temperature of the exposed portion of the PV panel during high insolation in day time increases to 100^0C, the TE modules attached to the back of the PV Panel would restrict the rise to a lower level, say 80^0C. This would in turn increase the efficiency of the PV system, and the hybrid system would produce additional energy through drawl of current from principles of the see-beck effect. The temperature of PV panel may be maintained through continuous removal of heat by the TEG.

4.3 MATLAB/Simulink modeling and simulation of hybrid PV-TE system

Fig.4.2 shows hybrid PV-TE system model a block of PV Panel and another of thermoelectric module. These are coupled in such a way that the solar insolation increases the temperature of the hotter side of the thermoelectric module. This rise in the temperature is in effect is the result of rising temperature on the surface of PV array. The control scheme eventually curbs the rise, lower the temperature gradient and finally stabilize it to a lower referenced level. To study the effect of the concept individual loads are connected to each module. The result depict the current output contribution of each module.

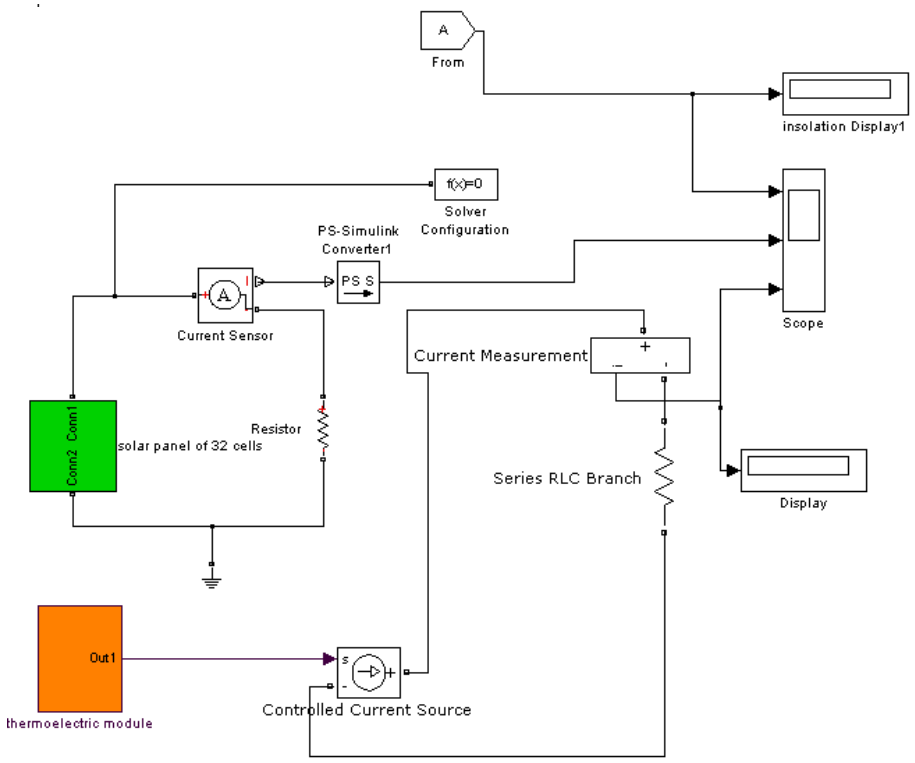

Fig 4.2 : Hybrid Photovoltaic and Thermoelectric generator system

4.4 Performance Evaluation of Hybrid system :

The Hybrid system shown in Fig.4.2 is operated with resistive load at the output terminals. Solar insolation is increased, in this setup, from zero to about 1500 W/m^2 which depicts the condition from day break till afternoon. As the insolation increases the temperature of the PV array will go on increasing till a saturation point is reached. The considered saturation point is 150^{0}C which corresponds to a solar insolation of 1000 W/m^2. Fig 4.3 shows the increase in current in Photovoltaic and Thermoelectric systems. The current in Photovoltaic system increases with increase in insolation till a max current is reached at an insolation of about 500 W/m^2, after this point the current increase is very slow manner as can be seen form Fig. 4.3. The current in thermoelectric module also increases with increase in temperature of the photovoltaic panel. It may be seen from Fig.4.3 that the current in thermoelectric module increases parabolically with the increase in temperature. At insolation of 1000 W/m^2 the temperature saturates and the output of the thermoelectric module becomes constant.

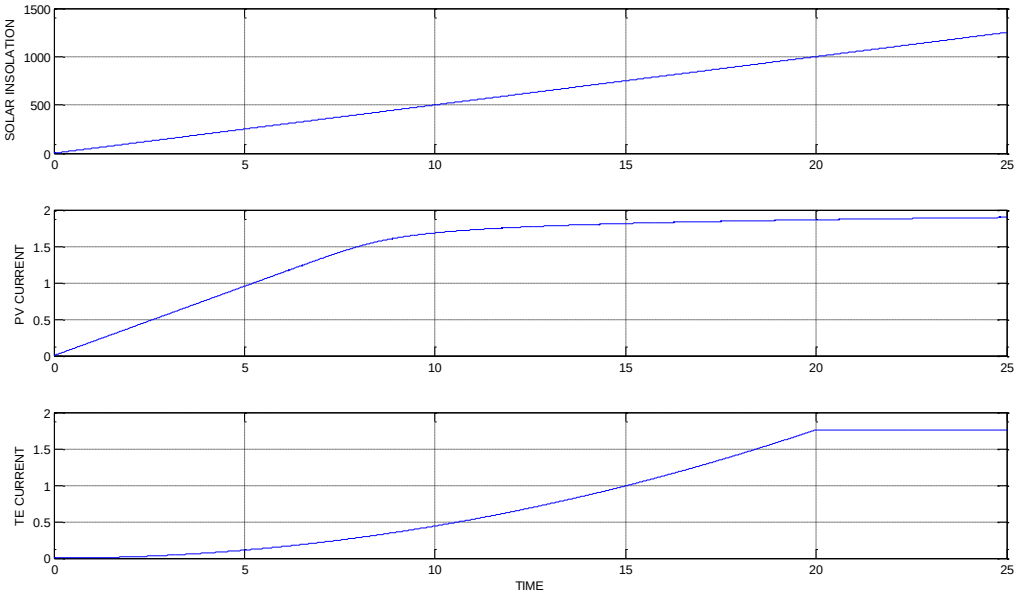

Fig 4.3 : Output of Hybrid PV-TE System

Chapter 5

Main Conclusion and Suggestions for future work

5.1 General

The main objective of the work has been to model a PV, TE and hybrid PV-TE water pumping system using solar power. The work has been carried out for modeling of solar Energy conversion system employing photovoltaic and thermoelectric cells as basic unit for the conversion system. The simulation of pumping system with vector control of pump/motor powered by photovoltaic generation has been successfully demontrated. The following are the main conclusions of the investigations carried out in this thesis work.

5.2 Main Conclusions

The performance of the water pumps connected to the photovoltaic systems both during steady state operation and transient operation has been investigated and demonstrated through MATLAB simulations.

Photovoltaic systems must be operated near the maximum power point to extract maximum energy from the system.

The heat produced by direct sunlight decreases the overall efficiency of the Photovoltaic system.

The efficient way of using this heat is by using thermoelectric conversion modules. The presented simulation results reveal the effectiveness of the proposed hybrid technique.

The number of TE modules must be increased to cover the total surface area on the back of PV panel for proper operation of the controller. These modules can be used for removing the heat and they are coined the name as *TE Coolers*.

Using vector control induction motor drive for pump operation the motor is started at low frequency decided by the controller and finally runs at the steady state condition at the set reference value of speed thus reducing the initial inrush current load on the Solar panel. When

the motor builds up the required starting torque to reach the set reference speed, the speed error reduces to almost zero rpm the winding current also reduces to the rated value and the developed torque becomes the load torque as observed in the starting response.

5.3 Suggestions for further work

- Experimentation of Standalone Water Desalination Using TE modules as coolers in Solar Water Desalination and Solar pumping for pumping needs, making the module useful for coastal areas & islands where grid electricity is not available.
- Experimentation of PV Panel where thermoelectric modules are used for generating power using extra heat ,in addition to cooling the concentrating solar panels.
- Cost analysis and payback period method for both systems (Hybrid & non Hybrid) in order to see which one is more preferable.
- Investigation in the quality of the electricity and heat produced by both systems
- Implementation of both systems in real life conditions and monitoring of their performance
- Large scale experiments, as well as experiments in a more controlled environment to determine which of the many physical processes involved has the greatest influence on the optimization of the systems
- Determination of the impact of the stack effect(Hybridizing) on the system.

REFERENCES

[1] H. Yamashita, K. Tamahashi, M. Michihira ,A. Tsuyoshi, K. Amako, and M. Park "A Novel Simulation Technique of the PV GenerationSystem using Real Weather Conditions" *Power Conversion Conference, 2002. PCC Osaka 2002*. Proceedings of the Volume 2, 2-5 April 2002 Page(s):839 - 844 vol.2

[2] P. P. Barker, J. M. Bing, "Advances in Solar Photovoltaic Technology: An Applications Perspective" at proceeding of *IEEE Power Engineering Society Summer Meeting – June 12-16, 2004, San Francisco, CA*

[3] Yuan. Li1, Taewon Lee, Fang. Z. Peng, and Dichen Liu "A Hybrid Control Strategy for Photovoltaic Simulator" *Applied Power Electronics Conference and Exposition, 2009. APEC 2009. Twenty-Fourth Annual IEEE* ,15-19 Feb. 2009 Page(s):899 – 903

[4] Jose A. Daminguez, Santiago Lorenzo, Jose M. Ruiz and Pablo Gutierrez. "Advanced Control for Pumping PV systems. INCA MODULES" *3rd world conference on photovoltaic energy conversion*, May 11-18 , 2003 Osaka, Japan.

[5] *C. Adnkne – J. Moncef , "*Modelling andsimulation of a PV-Inverter-Asynchronous motor Association in Photovoltaic Pumping Systems" *Power Engineering, 2001. LESCOPE '01. 2001 Large Engineering Systems Conference* on 11-13 July 2001 Page(s):146 - 151

[6] M. J. Case, E. E. Denny "A Novel Approach To Photovoltaic Powered Water Pumping Design" *Power electronics and motion control conference 2008, EPE-PEMC 2008* , 13th 1-3 Sept. 2008 Page(s):1798 - 1802

[7] N. Hamrouni, M. Jraidi, A. Cherif, A. Dhouib , "Measurements and Simulation of a PV Pumping Systems Parameters Using MPPT and PWM Control Strategies*" IEEE MELECON 2006*, May 16-19, Benalmádena (Málaga), Spain

[8] A. Zbeeb, V. Devabhaktuni, A. Sebak, and L. Maheshwari, "A New Microcontroller-based MPPT Algorithm for Photovoltaic Applications" *Proceedings of Internal Conference on Energy and Environment* March 19-21, 2009

[9] M. Chen, , L A. Rosendahl, T. J. Condra,J. K. Pedersen, "Numerical Modeling of Thermoelectric Generators With Varing Material Properties in a Circuit Simulator" *IEEE Transactions on Energy Conversion*, VOL. 24, NO. 1, March 2009

[10] H. Xiao, X. Gou and C. Yang "Simulation Analysis on Thermoelectric Generator System Performance" *System Simulation and Scientific Computing, 2008. ICSC 2008. Asia Simulation Conference - 7th International Conference* on 10-12 Oct. 2008 Page(s):1183 - 1187 2008 IEEE

[11] H.K.V. Lotsch, "Springer Series in optical sciences"

[12] David M. Rowe, University of Wales, Cardiff U. K. "CRC Handbook of Thermoelectrics"

[13] Dr. Bimal K. Bose "Modern Power Electronics and AC Drives"